Construction and Building Materials

Belite hydration at high temperature and pressure by in situ synchrotron powder diffraction

--Manuscript Draft--

Manuscript Number:	CONBUILDMAT-D-20-04874R2
Article Type:	Research Paper
Keywords:	Oil-Well-Cement; C−S−H conversion; belite reactivity; synchrotron radiation; Rietveld method; quantitative phase analysis
Corresponding Author:	Miguel A. G. Aranda Malaga, SPAIN
First Author:	Miguel A. G. Aranda
Order of Authors:	Miguel A. G. Aranda
	Alejandro Morales-Cantero
	Angeles G. De la Torre
	Ana Cuesta
	Edmundo Fraga-Lopez
	Shiva Shirani
Abstract:	Portland cements are currently used as Oil-Well-Cements for the sheath between the metal casing and the borehole. At high pressures and temperatures, the resulting C−S−H gel(s) is partly unstable and it can react to give different crystalline phases and changing microstructure which increases porosity. It is known that the addition of silica-rich materials to Portland cements, used to decrease the overall Ca/Si molar ratio, avoids/minimises the early strength retrogression experienced by neat cement slurries. Alternatively, belite-rich cement could be used but belite reactivity in these conditions is largely unexplored. Here, belite-rich mixtures have been quantitatively studied at 180 bars and of 160 ºC by in situ synchrotron powder diffraction using a tailored-designed spinning capillary cell. For model alite/belite mixtures, alite strongly accelerates belite hydration in these conditions. At 10 h of hydration, β-C 2 S shows a reaction degree of 30 and 80% for 20wt%C 3 S-80wt%C 2 S and 50wt%C 3 S-50wt%C 2 S mixtures, respectively. Furthermore, the 50wt%C 3 S mixture hydrates yielding significant amounts of Jaffeite and α-C 2 SH and the 20wt%C 3 S mixture gave no Jaffeite and much lower amount of α-C 2 SH. Finally, a belite cement has also been hydrated in these conditions and the reaction degree of belite was 50% at 10 h. The hydration of this cement did not yield Jaffeite neither α-C 2 SH in the studied experimental conditions.

Revised manuscript submitted to *Construction and Building Materials*

Belite hydration at high temperature and pressure by *in situ* synchrotron powder diffraction

Alejandro Morales-Cantero[1], Angeles G. De la Torre[1], Ana Cuesta[1], Edmundo Fraga-Lopez[2], Shiva Shirani[1], Miguel A.G. Aranda[1,*]

[1]*Departamento de Química Inorgánica, Cristalografía y Mineralogía, Universidad de Málaga, Málaga, 29071, Spain.*

[2]*ALBA Synchrotron, Carrer de la Lum, 2-26, 08290 Cerdanyola del Vallès, Barcelona, Spain.*

* *email: g_aranda@uma.es*

Abstract.

Portland cements are currently used as Oil-Well-Cements for the sheath between the metal casing and the borehole. At high pressures and temperatures, the resulting C–S–H gel(s) is partly unstable and it can react to give different crystalline phases and changing microstructure which increases porosity. It is known that the addition of silica-rich materials to Portland cements, used to decrease the overall Ca/Si molar ratio, avoids/minimises the early strength retrogression experienced by neat cement slurries. Alternatively, belite-rich cement could be used but belite reactivity in these conditions is largely unexplored. Here, belite-rich mixtures have been quantitatively studied at 180 bars and of 160 ºC by *in situ* synchrotron powder diffraction using a tailored-designed spinning capillary cell. For model alite/belite mixtures, alite strongly accelerates belite hydration in these conditions. At 10 h of hydration, β-C_2S shows a reaction degree of 30 and 80% for 20wt%C_3S-80wt%C_2S and 50wt%C_3S-50wt%C_2S mixtures, respectively. Furthermore, the 50wt%C_3S mixture hydrates yielding significant amounts of Jaffeite and α-C_2SH and the 20wt%C_3S mixture gave no Jaffeite and much lower amount of α-C_2SH. Finally, a belite cement has also been hydrated in these conditions and the reaction degree of belite was 50% at 10 h. The hydration of this cement did not yield Jaffeite neither α-C_2SH in the studied experimental conditions.

Keywords: Oil-Well-Cement, C–S–H conversion, belite reactivity, synchrotron radiation, Rietveld method, quantitative phase analysis

1. Introduction.

Oil-Well-Cement (OWC) is a special kind of cement [1,2] used for specific applications mainly in oil, gas and geothermal industries. Furthermore, in the last two decades, there has been increased interest in oil and gas extraction from unconventional resources like shale gas and heavy oil. The pastes derived from OWC are subjected to variable conditions including high pressures (up to 1000 bar) and high temperatures (up to 300°C). Consequently, the hydration processes change substantially, and the hydration phases formed under these conditions are different (or they can be) than those obtained at room temperature and atmospheric pressure [3].

The hydration of PC close to ambient conditions is widely studied and it mainly consists of two different types of reactions which can interact with each other. These are the silicate and the aluminate reactions [4] (cement notation for the different phases will be used hereafter). The main silicate reaction consists of the dissolution of alite (simplified as Ca_3SiO_5 or C_3S), supersaturation of the pore liquid with the different ionic species and then, the crystallization of portlandite, $Ca(OH)_2$ and the precipitation of a nanocrystalline calcium-silicate-hydrate (C–S–H) gel which the following average stoichiometry at the microscale, $(CaO)_{1.8}SiO_2{\cdot}4H_2O$ [5]. The hydration reaction of belite seems to be similar to that of alite, although the reactivity of belite (simplified as Ca_2SiO_4 or C_2S) is much slower, and it is assumed to yield an analogous C–S–H gel. Aluminate reactions mainly consist on the dissolution of aluminates, i.e. C_3A and C_4AF and calcium sulfate sources yielding crystalline ettringite and AFm phases at room pressures.

The hydration reactions of cements can change at high pressures and temperatures (HPHT) and the hydrated phases can be partly different from those obtained at room temperature and pressure [6,7]. Reports dealing with different cement systems [7–9] have shown that the effect of temperature is larger than that of pressure. For instance, it was reported that C–S–H gel was not fully stable at high temperature [10], and hence, that non-ambient conditions led to its partial decomposition/reaction to yield other (crystalline) hydrates, such as α-C_2SH and/or Jaffeite, $C_6S_2H_3$ [10,11]. Because the Ca/Si ratio of Jaffeite is similar to that of alite, it could readily form at HPHT. At high temperatures, pressure should favour the appearance of phases with higher mass densities, i.e. smaller molar volumes. In such conditions, α-C_2SH stability will be favoured respect to that of Jaffeite. The transformation to higher density phases increases the porosity and decreases the mechanical strength (behaviour known as strength retrogression) [12–18]. Moreover, C–S–H gel crystallization at HPHT has been reported to yield tobermorite and related minerals [19–22] and to change its microstructure by densification and hence porosity increase [22,23]. All these processes lead to early strength retrogression by neat cement slurries cured at HPHT. The addition of silica-rich compounds to Portland cement decreases the Ca/Si ratio and it mitigates this undesired conversion [2,24]. Therefore, there are many publications dealing with the addition of silica fume (SF), metakaolin (MK), quartz with small particle sizes, or fly ash (FA) to OWC to decrease the Ca/Si ratio of the resulting binder [23,25–27].

In situ characterization is very useful to understand the hydration under these conditions but most HPHT diffraction studies reported qualitative or semi-quantitative results mainly devoted to the hydration of C_3S [6,7,10,28]. The lack of quantitative information on the coupled role of pressure and temperature is due to the lack of suitable tools to carry out high-resolution phase-selective *in situ* studies during cement hydration. In order to address this knowledge gap, we have recently developed a HPHT capillary cell which allows rotation to improve the powder averaging [29]. The possibility of rotation coupled with synchrotron X-rays allowed to quantitatively follow *in-situ* OWC hydration reactions. Furthermore, a very recent work [30] performed an *in situ* synchrotron powder diffraction study to follow the reaction of each phase in an OWC paste at 150 bars and

150ºC. Without the use of admixtures, the reaction degree of alite reached 90% after 7 h and that of belite was 42% at 14 h.

As current OWC are based on Portland cements, retardants are commonly needed to slow down alite reaction allowing enough open time for correct paste pumping and placement [31]. Furthermore, as the Ca/Si is close to 3/1, silica-rich supplementary cementitious materials like SF, MK or FA, are used to decrease this ratio in the final hydrate assemblage. An alternative approach could be to use belite cements as Oil Well Cements. In addition to the benefit due to the possible avoidance of porous development, CO_2 footprint reduction will be attained. However, belite reactivity is very much unexplored under these conditions. Furthermore, an additional advantage of this type of cements is the low heat of hydration for drilling in permafrost area. Heat of hydration of Portland cement can cause melting of surrounding permafrost, hence every effort to minimize this is worth to be researched.

The objective of this work is to study belite reactivity at high temperature and pressure. In order to do so, *in-situ* synchrotron powder diffraction data have been collected in model C_3S-C_2S mixtures at 180 bars and 160ºC. Furthermore, an industrially-fabricated belite cement has also been studied under similar conditions. This study profits from the recent development of the HPHT spinning capillary cell.

2. Materials and Methods.

2.1. Materials.

Three single phases were used in this study. I) Crystalline I_2 (extra pure resublime quality) was purchased from Scharlen. II) Triclinic tricalcium silicate, t-C_3S, was purchased from Mineral Research Processing (M.R.PRO). III) Dicalcium silicate, β-C_2S, with $Ca_2Si_{0.972}Al_{0.028}O_{3.986}\square_{0.014}$ stoichiometry was synthetized with the aluminium content that allows to stabilize the β–polymorph [32].

β-C_2S was synthetized as follows. SiO_2 (Alfa Aesar, 99.5%), $CaCO_3$ (Alfa Aesar, 99.95-100.05%) and γ-Al_2O_3 (Alfa Aesar, 99.999%) were used as raw materials in the stoichiometric proportions given above. Raw materials were mixed in a Micro-deval mill (Proeti) for 30 minutes. Then, the powder was preheated for 4 h up to 1050ºC with a heating rate of 10 ºC/min. The material was grinded for 45 min using the Micro-deval device to obtain a better homogenization. Later, the material was pressed into pellets and heated up to 1500ºC for 6 h. The material was quenched from high temperature with an air flow. The resulting pellets were grinded in a disk mill (Siebtchnik). Again, new pellets were prepared, heated up to 1200ºC for 1 h with a heating rate of 20 ºC/min, quenched with an air flow and grinded in the disk mill. Then, an additional cycle was carried out. New pellets were prepared and finally heated up to 1000ºC for 30 min and cooled with liquid nitrogen. These pellets were grinded in the disk mill.

An industrially prepared Belite cement, BC, (type CEM I 42.5 N) from Buzzi Unicem SpA was also used [33]. This material was characterized as reported below and it had a Blaine value of 5023 cm^2g^{-1}.

The hydration of the samples was performed by adding the required amount of water to the powder samples. The water to cement (w/c) mass ratio used was 0.50 for the BC sample and 0.45 for the t-C_3S and β-C_2S series. The pastes were manually stirred in a plastic beaker for 2 min to ensure homogenization. A paste was immediately loaded, with the aid of a syringe and a short piece of silicone tube, into the sapphire capillaries (Saint-Gobain crystals) with an outer diameter of 3.18

mm and inner one of 1.75 mm. PTFE cylindrical plugs of 3 mm of length and 1.75(5) mm of diameter were used to block both ends of the sapphire capillaries at least at 10 mm from the end of the capillary. These PTFE plugs allow the pressure to be transmitted to the paste meanwhile they avoid the direct contact of the oil with the hydrating paste.

2.2. Methods.

2.2.1. Laboratory X-ray powder diffraction (LXRPD).

LXRPD data for anhydrous materials were collected on a D8 ADVANCE (Bruker AXS) diffractometer (SCAI – Universidad de Málaga) equipped with a Johansson monochromator, using strictly monochromatic Mo-Kα_1 radiation, λ=0.7093 Å, in transmission geometry (θ/θ).

2.2.2. Synchrotron X-ray powder diffraction (SXRPD) experiment.

Full details about the beamline, capillary cell and experimental conditions have been very recently reported [29,30,34]. A photon energy of 19.7 keV, λ=0.62820(1) Å, was selected with a Si(111) channel-cut monochromator to collect powder diffraction data in Debye-Scherrer configuration. The beam size was 0.6 mm vertical and 0.8 mm horizontal. The detector was a LX255-HS Rayonix CCD placed at 306.65 mm from the sample (tilt vertical angle of 27.335º). These values were determined for the final configuration using quartz as an external standard.

A sapphire capillary filled with quartz was used as the standard to calibrate the detector setup and another filled with iodine was used to determine that the target pressure and the pressure within the capillaries were the same. The sapphire capillaries containing the paste were blocked with the PTFE plugs and loaded into the spinning capillary cell. Firstly, the static pressure was manually generated by a pump generator to achieve 180 bars. Immediately, the heating system was turned on to reach 155-160ºC. Hence, target pressures and temperatures were reached at slightly different times for each sample. As the influence of temperature in the hydration reactions is larger than that of pressure, always high pressure was reached first. The zero time, for all reported HPHT hydration studies described hereafter, is that when the target temperature was reached.

The cell was rotated at 30 rpm (60 rpm for the iodine and BC experiments). It contains a Micos LS-180 translation stage that enables to collect 2D data in any desired horizontal point of the capillary. For the studied samples, 5 snapshots were taken at different positions along the capillary, at 0.5 mm intervals with an exposure time of two seconds per snapshots (1 snapshot and 10 seconds of exposure for the iodine). Patterns were collected with intervals of ~15 min. The 2D images were reduced to 1D data by pyFAI software [35]. An empty sapphire capillary was firstly analysed and the spots from the sapphire capillaries were masked during the integration step. Five 1D raw patterns were collected at different capillary positions and then sum up with a local software yielding the final 1D dataset to be analysed by Rietveld methodology.

2.2.3. LXRPD and SXRPD data analysis.

GSAS suite of programs [36] was used to analyse the powder patterns by Rietveld methodology. Background coefficients, zero-shift error, cell parameters and peak shape parameters (using a pseudo-Voigt function) were refined [37].

2.2.4. Particle size distribution (PSD) analysis.

The average particle size distribution of the anhydrous samples was measured by laser diffraction (Malvern MasterSizer S, UK). The powders were previously dispersed in isopropanol using an ultrasonic bath.

2.2.5. BET surface area determination.

The specific surface areas of the selected samples were measured by multi-point N_2 adsorption with a BET (ASAP 2420, Micromeritics, USA) instrument.

2.2.6. X-ray fluorescence (XRF) analysis.

The elemental composition of BC was measured by XRF using an ARL ADVANT'XP+ (Thermo Fisher) equipment at the SCAI – Universidad de Málaga.

3. Results and discussion.

3.1. Anhydrous sample characterization

Crystalline Iodine was used to test that the applied pressures reached the samples within the capillaries, which were isolated from the pressure transmitting oil by the PTFE cylindrical plugs. The LXRPD Rietveld fit for this crystalline standard is shown in Fig. S1. Preferred orientation effect was observed in the pattern and it was corrected by the March-Dollase approach [38].

Triclinic tricalcium silicate sample was initially characterized by laboratory techniques. Its PSD is displayed in Fig. S2a having a $d_{v,50}$ of 4.6 μm and the BET specific surface area of 1.87(1) m^2/g. The Rietveld fit of the LXRPD data for t-C_3S showed that it was a single crystalline phase, see Fig. S3. Beta dicalcium silicate sample was also analysed by laboratory tools. Fig. S2b displays its PSD ($d_{v,50}$=2.4 μm), and the BET area was 2.25(1) m^2/g. Fig. S4 displays the Rietveld fit for this sample showing that it was also a single phase.

The industrially-produced BC was characterized by LXRPD and XRF. Fig. S5 displays the Rietveld fit for this sample which yielded the Rietveld quantitative phase analysis reported in Table S1. The elemental analysis determined by XRF is given in Table S2. Fig. S2c displays the PSD ($d_{v,50}$=7.5 μm) for this cement which has a BET area of 1.40(1) m^2/g.

3.2. Model samples at high pressure and temperature

Firstly, the set up was tested using I_2 powder within a sapphire capillary to ensure that the system works correctly and chiefly, that the PTFE plugs transmitted the loaded pressure. Crystalline I_2 was selected due to its large compressibility with a Bulk modulus value of 7.7 GPa. Synchrotron powder patterns were collected at room pressure and 50, 100, 150 and 185 bars on loading and unloading waiting for 10 minutes before data acquisition for sample/system stabilization. Fig. S6 (top) shows the Rietveld fit for the data taken at 185 bars as an example of the quality of the data that can be obtained. The unit cell values for I_2 decreased with pressure and then increased with releasing pressure, as expected. Fig. S6 (bottom) displays the fit of these data to the second-order (K'=4.0) Birch-Murnaghan equation of state that allows obtaining the bulk modulus. The obtained values where 6.2 GPa and 8.3 GPa with increasing and decreasing pressure, respectively. The closeness of these values, taking into account the limited pressure range, to the reported bulk modulus of I_2 allows to state that the pressure is correctly transmitted by the PTFE plugs.

The hydration reaction of t-C_3S (w/c=0.45) was followed up to 2.1 h at 180 bars and 160ºC. As described in the method section, the pressure was increased first and then the temperature was raised. This full process took 32 minutes after paste mixing and this point in time is defined as t_0. This is the procedure used hereafter which means that for this sample, t_0 took place 32 minutes after water-cement mixing. With this consideration for the time origin of the experiment, Fig. 1 displays the time evolution for the *in situ* 1D SXRPD patterns for the t-C_3S paste at HPHT. In the pattern collected at 5 minutes, 0.1 h, the main diffraction peak of portlandite, located at 7.3º (2θ), is hardly visible which means that hydration reaction rate before t_0 was (very) small. Qualitatively, it can be stated that C_3S hydration in these conditions is very fast as the intensities of the diffraction peaks

strongly decrease in just two hours in agreement with a previous report [39]. It is also shown that Jaffeite phase starts to form after 1 hour of hydration.

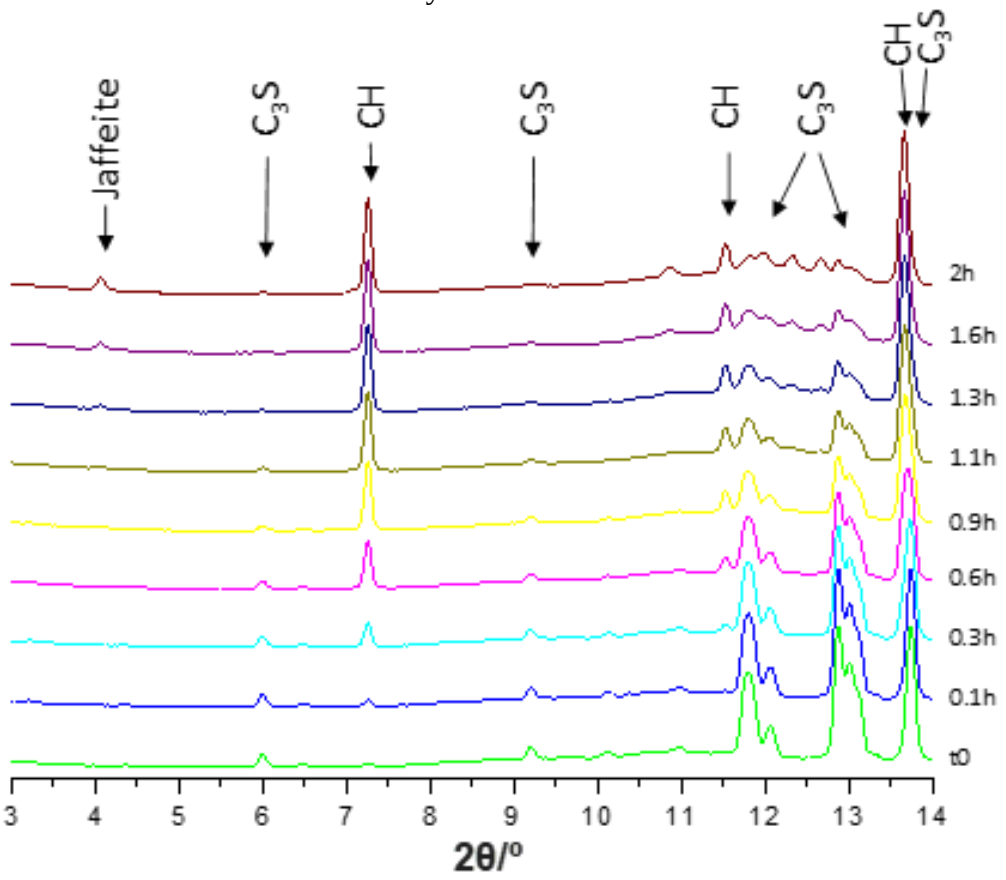

Fig. 1. *Selected low angle range of the SXRPD raw patterns, λ=0.6282 Å, for the t-C_3S paste collected at 180 bars and 160ºC as a function of hydration time. The main diffraction peaks due to a given phase are labelled.*

The *in situ* synchrotron powder diffraction patterns were analysed by Rietveld methodology [40]. However, this study has been carried out without using an internal standard [41] which would allow obtaining the overall amount of amorphous content [42]. This procedure has not been carried out as the addition of the standard at high temperature and pressure could affect the hydration reaction mechanisms and rates. Here, an alternative approach has been employed benefiting from the fact that the same capillary is studied with the same overall amount of material and with the same incoming X-ray flux. Hence, the histogram scale factor is kept constant and the analysis is derived from the evolution of the phase scale factors. Fig. S7 displays two Rietveld plots for hydrating t-C_3S at HPHT and selected hydration times (t_0 and 2 h) as representative examples. The Rietveld analysis of the patterns yielded the phase scale factors for t-C_3S, CH and Jaffeite which are reported in Table S3. From the evolution of the phase scale factor for t-C_3S, its degree of reaction can be accurately derived which is shown in Fig. 2. It is highlighted that the hydration rate of t-C_3S is very fast in these HPHT conditions reaching 90% reaction degree in just two hours.

The hydration of β-C_2S paste (w/c=0.45) was studied at 180 bars and two temperatures 120 and 160ºC. Unfortunately, due to instabilities in the temperature control (with variations larger than 20ºC) the SXRPD data collected close to 160ºC could not be used and therefore the data are not reported here. After this measurement was stopped, the problem was identified as a poor electrical connection to the Eurotherm Nanodac controller of the cell which was fixed. For the study at T=120ºC, t_0 took place 44 minutes after paste mixing. Fig. S8 shows 1D SXRPD patterns for β-C_2S

pastes during the first 7 hours of hydration at 180 bars and 120ºC. It is clear that single phase β-C_2S does not hydrate at 120 ºC and 180 bars in 7 hours. Consequently, the Rietveld study was not performed for these patterns.

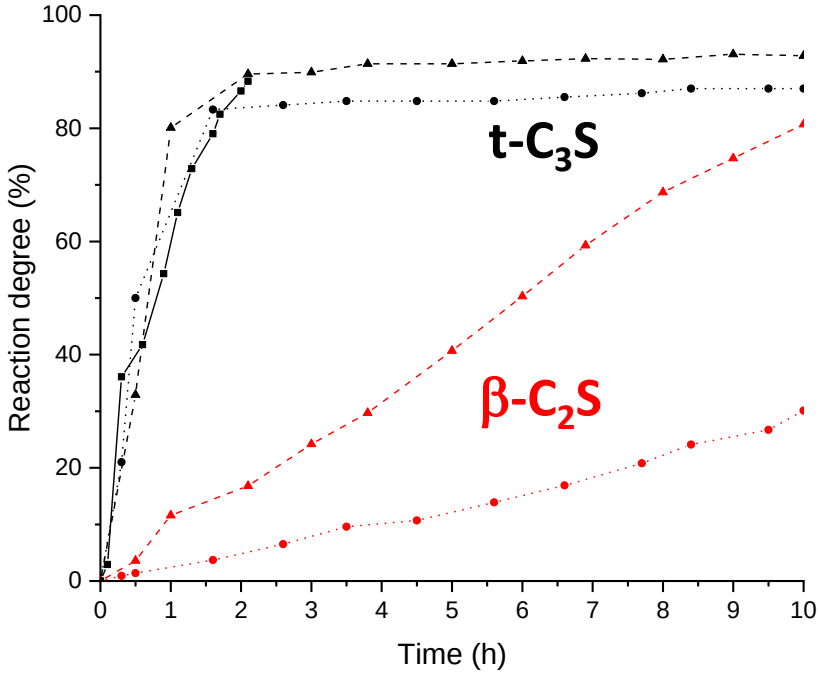

Fig. 2. *Evolution of the degree of reaction for the t-C_3S (black symbols) and β-C_2S phases (red symbols) with time at 180 bars and 160ºC in the three model pastes studied here: (i) 100 wt% of t-C_3S (squares); (ii) 50 wt% of t-C_3S and 50 wt% of β-C_2S (triangles); and 20 wt% of t-C_3S and 80 wt% of β-C_2S (circles).*

In order to study the effect of C_3S on the hydration rate of C_2S, the hydration of two model mixtures at 180 bars and 160ºC were studied. The prepared mixtures were 50 wt% t-C_3S and 50 wt% β-C_2S (50C_3S-50C_2S) and 20 wt% t-C_3S and 80 wt% β-C_2S (20C_3S-80C_2S). For 50C_3S-50C_2S, the target pressure and temperature were reached 55 minutes after mixing. Fig. 3 shows the *in situ* 1D SXRPD patterns for this paste at selected ages of hydration to qualitatively show the phase evolution. At 1 h, there is an important amount of portlandite formed as deduced from the intensity of its main diffraction peak situated at 7.3º (2θ). The formation of Jaffeite is also clearly visible at this hydration time, diffraction peak at 4.1º (2θ). Moreover, the amount of t-C_3S is very small at 1 h of hydration and almost negligible at 2 h. On the other hand, the main diffraction peaks of β-C_2S strongly decreased from 1 h to the end of the experiment at 10 h of hydration. It is worth noting the appearance of α-C_2SH at ~3 h of hydration was concurrent with the hydration of β-C_2S, and the intensities of their diffraction peaks increased with the hydration age. These patterns were analysed by the Rietveld methodology and two Rietveld plots, at ~0.5 and ~9 h of hydration, are shown in Fig. 4 as examples of the quality of the fits that it can be obtained with the setup developed at ALBA synchrotron [29,30]. The scale factors of the different phases and degree of reaction for the anhydrous phases are given in Table S4. Fig. 2 also shows the evolution of the degree of reaction for t-C_3S and β-C_2S with time. It is underlined that β-C_2S is the same powder used above which did not react at 7 h at P=180 bars and T=120 ºC. However, the high pH from alite dissolution activates belite reaction which was 80% at 10 h (at P=180 bars and T=160 ºC).

A similar study was carried for the 20C_3S-80C_2S mixture, hydrated also at 180 bars and 160ºC. Due to some technical difficulties, the target pressure and temperature were reached 1 h and 27 min after

mixing. Fig. 5 shows the *in situ* 1D SXRPD patterns for this paste at selected hydration ages. Portlandite starts to crystallize at very early ages concurrent with the dissolution of t-C_3S, as expected. At 2.6 h of hydration this phase reaches its maximum and its content remains constant within the error of the analyses. Jaffeite crystallization is hardly visible for this mixture. The qualitative inspection of the dissolution rate of β-C_2S for this sample shows that it is much slower than that shown for the 50C_3S-50C_2S paste, see Fig. 3. These patterns were analysed by the Rietveld methodology and two Rietveld plots, at t_0 and ~8.4 h, are displayed in Fig. S9 as representative examples. Table S5 reports the scale factors of the different crystalline phases and degree of reaction for t-C_3S and β-C_2S. Fig. 2 also shows the time evolution of the degree of reaction for the two anhydrous phases in this mixture. It is noteworthy that C_3S has reacted ~80% at 2 h but β-C_2S hydration rate is much smaller than that of belite in the 50C_3S-50C_2S in exactly the same experimental conditions. This seems to indicate that not only the pH value but the overall amount of $Ca(OH)_2$ is key for belite activation. Furthermore, for this belite-rich mixture at 10 h of hydration, Jaffeite formation is not observed, as hypothesized, and the content of α-C_2SH is rather small, see Fig. 5.

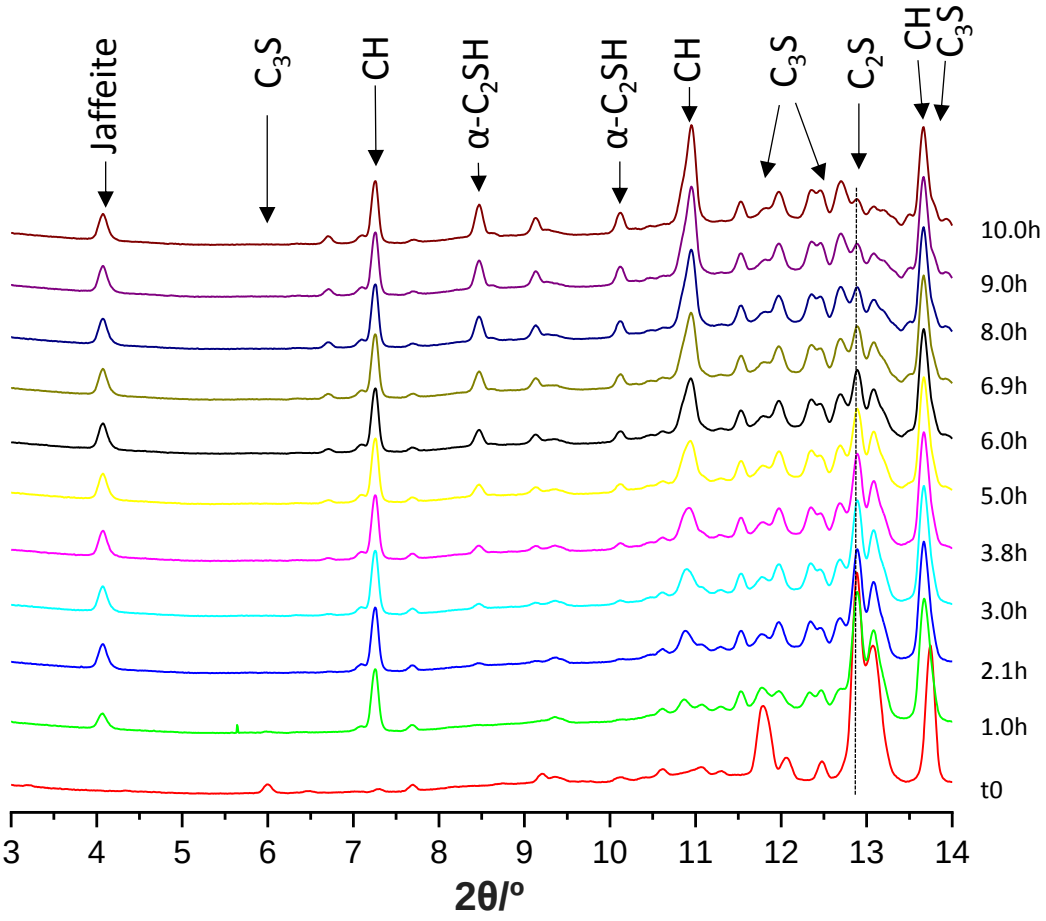

Fig. 3. *Selected low angle range of the SXRPD raw patterns, λ=0.6282 Å, for the 50 wt% t-C_3S and 50% β-C_2S paste collected at 180 bars and 160ºC as a function of hydration time. The main diffraction peaks due to a given phase are labelled.*

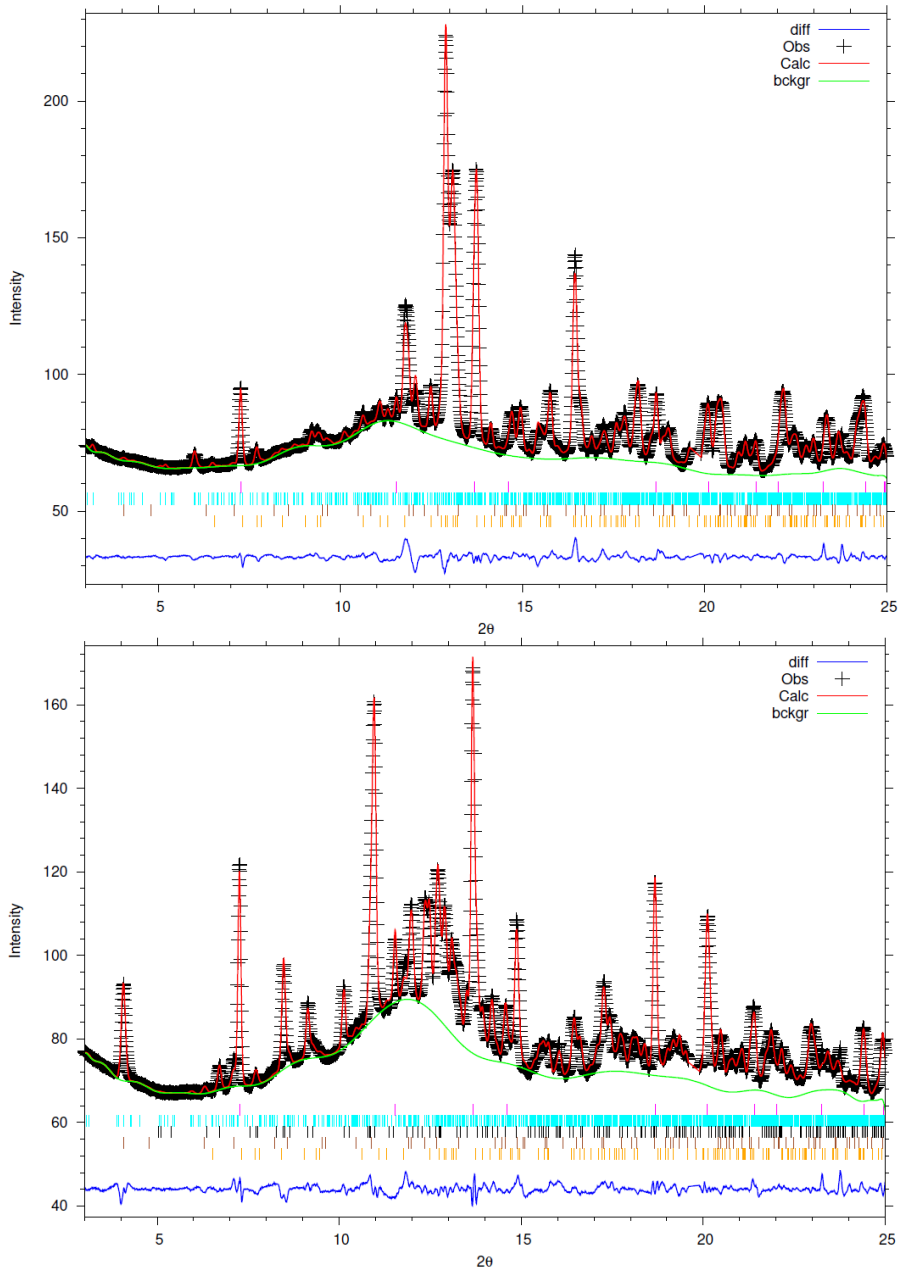

Fig. 4. *In situ SXRPD Rietveld plots, λ=0.6282 Å, for 50 wt% t-C_3S and 50 wt% β-C_2S paste hydrating under 180 bars and 160ºC at (top) 0.5 hours and (bottom) 9 hours of hydration. Because the same capillary is scanned at different hydration times, the diffraction intensities (and the background level for C-S-H development) can be directly compared.*

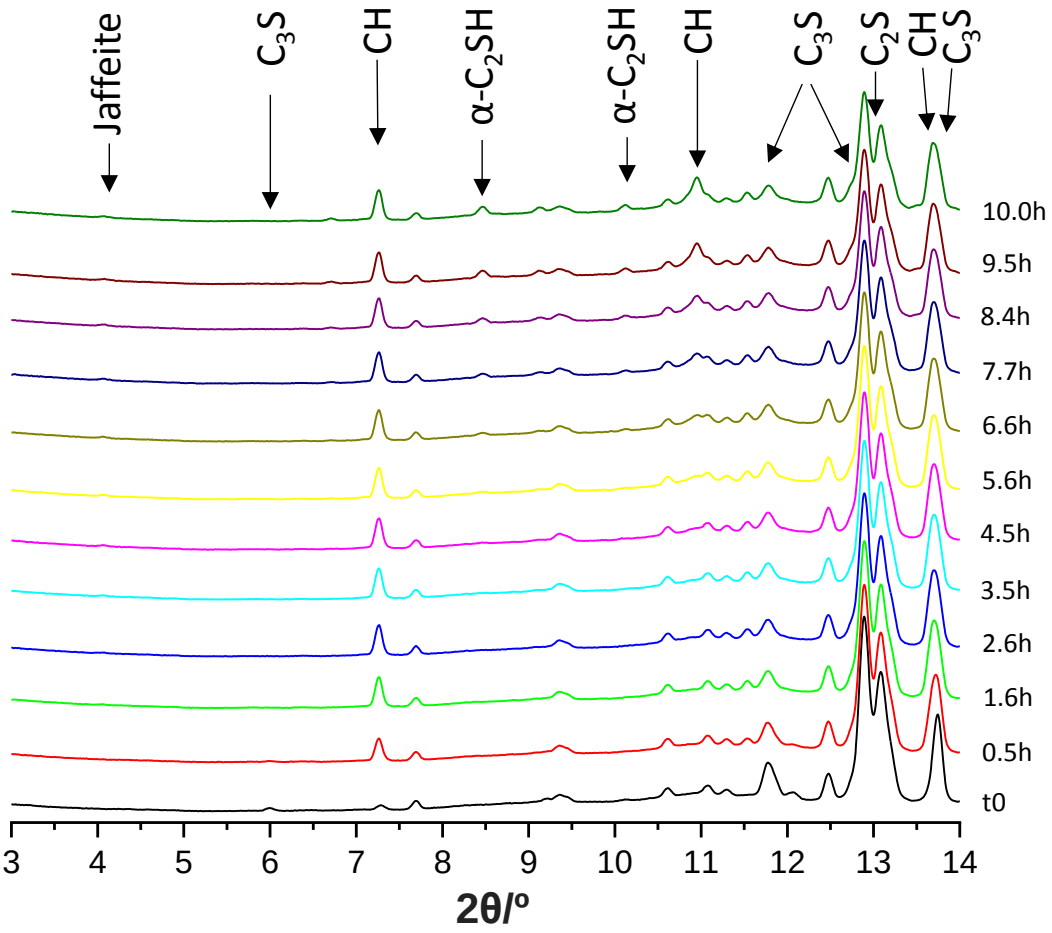

Fig. 5. *Selected low angle range of the SXRPD raw patterns, λ=0.6282 Å, for the 20 wt% t-C_3S and 80% β-C_2S paste collected at 180 bars and 160ºC as a function of hydration time. The main diffraction peaks due to a given phase are labelled.*

3.3. Belite cement hydration at high pressure and temperature.

The hydration behaviour for the employed BC was studied up to 14 h using w/c=0.50 under 180 bars and 155ºC. For this sample, the target pressure and temperature were reached 55 minutes after mixing. Fig. 6 displays the *in situ* 1D SXRPD patterns as a function of the hydration time. An initial reaction, in the time elapsed between mixing and HPHT stabilization, took place. The first *in situ* SXRPD patterns, taken at 0.1 h, shows that a small fraction of ettringite (AFt) was already form ed (see its main diffraction peak located at 3.7º (2θ)). It can be also observed that this phase rapidly decomposes at HPHT and its content is negligible at 1.2 h of hydration, in agreement with a previous report [30]. For this BC sample, the formation of katoite, whose main reflection is located at 7.1º (2θ), appears at 1.2 hours of hydration and its amount seems to be constant up to 14 h. The main diffraction peak of portlandite, located at 7.3º (2θ), reaches its maximum close to 3 h, in line with the alite hydration rate as its dissolution seems to stop at ~3 h. Meanwhile, the dissolution of β-C_2S is slower but it continues along the full duration of the experiment. Selected patterns were analysed by the Rietveld methodology and Fig. S10 displays two selected Rietveld plots at ~1.2 and ~14 h of hydration. The scale factors obtained from the Rietveld fits are reported in Table S6. Moreover, the evolution of the degree of reaction with time for t-C_3S and β-C_2S, calculated assuming the start of the phase dissolution at the earliest pattern, t=0.1 h, is displayed in Fig. 7.

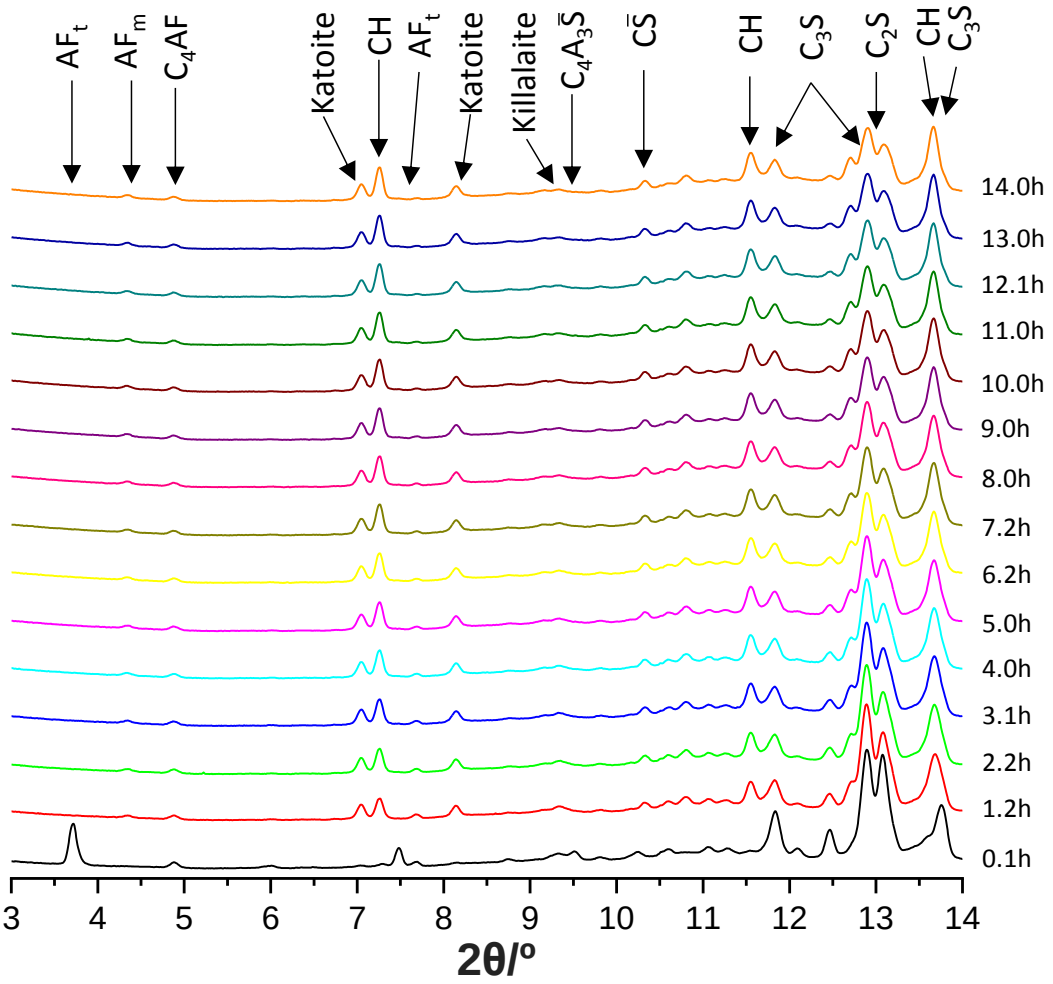

Fig. 6. *Selected low angle range of the SXRPD raw patterns, λ=0.6282 Å, for the belite cement paste collected at 180 bars and 155ºC as a function of hydration time. The main diffraction peaks due to a given phase are labelled.*

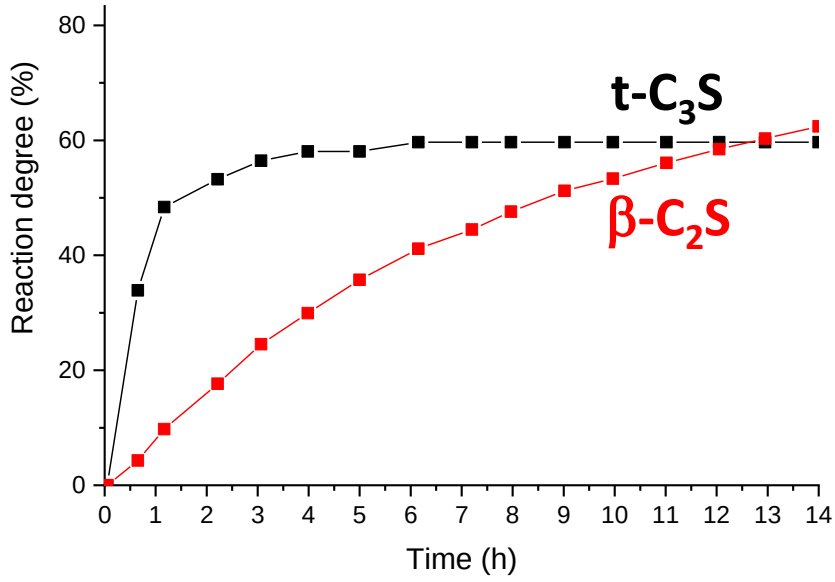

Fig. 7. *Evolution of the degree of reaction for the t-C_3S (black squares) and β-C_2S (red squares) phases with time at 180 bars and 155ºC for the belite cement paste.*

3.4. General discussion.

Due to a technical problem with the *in situ* cell, the β-C_2S dissolution at 180 bars and 160ºC could not be measured. However, this material when hydrated as a single phase does not dissolve at all at 180 bars and 120ºC up to 7 h, see Fig. S8. Hence, it could be anticipated that its dissolution rate should be small at the same pressure and 160 ºC. On the other hand, at P=180 bars and T=160 ºC, phase pure t-C_3S hydrates ~90% in 2 h. Furthermore, Fig. 2 shows that the presence of C_2S slightly delays hydration rate of C_3S. At 7 h of hydration, C_3S has a reaction degree of 86 and 92% in the $20C_3S$-$80C_2S$ and $50C_3S$-$50C_2S$ mixtures, respectively. This effect is presently not understood and we speculate that it could be due to a lack of water for the final stages of the hydration reactions. However more research is needed to shed light about this behaviour. Conversely, the presence of C_3S strongly accelerates the hydration of C_2S. At 10 h of hydration at this HPHT conditions, β-C_2S shows a reaction degree of 30 and 80% for $20C_3S$-$80C_2S$ and $50C_3S$-$50C_2S$ mixtures, respectively. Our results indicate that both a high pH and a large reservoir of $Ca(OH)_2$ in the hydrating paste seem to be key for belite activation. Furthermore, we speculate that, under these experimental conditions, single belite phase will hydrate faster if plain water is replaced by calcium hydroxide saturated water. However, we are aware of a work showing a decrease of the dissolution rate of β-C_2S with the increase of calcium hydroxide concentration at very early hydration ages, less than one hour [43], at room temperature and pressure. Therefore, more research is needed to firmly establish the dependence of belite hydration kinetics with the $Ca(OH)_2$ concentration at HPHT conditions.

Jaffeite is a high pressure phase and its formation has been widely reported from the reaction of C–S–H gel and portlandite [10,14,26,39]. However, the formation mechanism is complex as pure C_3S paste showed a very large degree of reaction but Jaffeite formation was moderate. The $50C_3S$-$50C_2S$ paste showed the largest fraction of Jaffeite formation. Moreover, in this mixture, also a large amount of α-C_2SH was measured and its development took place at the same time than belite dissolution. However, our diffraction data does not allow to conclude if α-C_2SH is formed directly from belite dissolution or if C–S–H formation is needed as an intermediate step. More research is needed to clarify this point.

One industrially-produced belite cement(type CEM I 42.5 N) has been studied under these HPHT conditions. The cement contained 54 wt% of belite and 25 wt% of alite, see Table S1. Its PSD profile is given in Fig. S2c showing 7.5 and 38 μm for $D_{v,50}$ and $D_{v,90}$, respectively. Alite reacts very fast at the starting of the experiment reaching a reaction degree close to 60% at 3 h and its dissolution ceased. This striking observation is not in disagreement with the data reported in Fig. 2, where alite reaction degrees were ~90% at 10 h because the alite particle size for that sample was likely smaller, see Fig. S2a with 4.6 and 11 μm for $D_{v,50}$ and $D_{v,90}$, respectively. Chiefly, the belite reaction degree in the belite cement increases smoothly, see Fig. 7, reaching 62% at 14 h of hydration slightly larger than that of alite at that hydration time, 60%. Acknowledging that this experiment has a very particular set of conditions, it is really noteworthy to find a hydration time where belite reaction degree is larger than that of alite. These results are likely due to hydration inhibition of big alite particles at large degree of reaction. We speculate that the origin of the unhydrated C_3S, about 7 wt%, is likely the lack of available water close to the partly reacted alite particles. This is an indirect consequence of the major consumption of the added water, w/c=0.50, by the hydration of the phases of this cement with smaller particle sizes. However, more research is needed to clarify this point.

4. Conclusions

This *in situ* synchrotron study, using a high-pressure high-temperature spinning capillary cell operated at 180 bars and of 160ºC, has allowed extracting the following main conclusions:

1. Alite reacts very fast in these conditions reaching 85-90% degree of reaction at 2 h for a pure phase experiment as well as for alite-belite mixtures. Belite slightly delays alite hydration rate.

2. Belite hydration rate is strongly accelerated by alite presence. At 10 h, β-C_2S has a reaction degree of 30 and 80% for mixtures with 20 wt% and 50 wt% of C_3S, respectively.

3. The 50wt% mixture of alite and belite develops significant amounts of Jaffeite, $C_6S_2H_3$, and α-C_2SH. Conversely, the mixture of 20 wt% of alite and 80 wt% of belite does not yield Jaffeite and the amount of α-C_2SH is comparatively smaller.

4. The belite degree of reaction of an industrially produced belite cement reached 62% at 14 h of hydration slightly larger than that of alite, 60%.

Acknowledgement. This work has been supported by BIA2017-82391-R research grant, which is co-funded by FEDER. We thank ALBA synchrotron for providing beam time at NCD-Sweet beamline and Marc Malfois for his assistance during the experiment. We also thank Buzzi Unicem SpA for providing us with more than 30 kg of a large-scale production belite cement.

Data availability. All *in situ* synchrotron X-ray powder diffraction patterns analysed in this article can be freely accessed on Zenodo at https://doi.org/10.5281/zenodo.3744210, and used under the Creative Commons Attribution license.

References

[1] F.M. Lea, P.C. Hewlett, Lea's chemistry of cement and concrete, Elservier Butterworth-Heinemann, 2001.

[2] E.B. Nelson, D. Guillot, eds., Well Cementing, 2nd ed., Schlumberger, 2006.

[3] H.F.W. Taylor, Cement chemistry. 2nd ed., Acad. Press. 20 (1997) 335. https://doi.org/10.1016/S0958-9465(98)00023-7.

[4] K.L. Scrivener, P. Juilland, P.J.M. Monteiro, Advances in understanding hydration of Portland cement, Cem. Concr. Res. 78 (2015) 38–56. https://doi.org/10.1016/J.CEMCONRES.2015.05.025.

[5] A. Cuesta, J.D. Zea-Garcia, D. Londono-Zuluaga, A.G. De La Torre, I. Santacruz, O. Vallcorba, M. Dapiaggi, S.G. Sanfélix, M.A.G. Aranda, Multiscale understanding of tricalcium silicate hydration reactions, Sci. Rep. 8 (2018) 8544. https://doi.org/10.1038/s41598-018-26943-y.

[6] A.C. Jupe, A.P. Wilkinson, G.P. Funkhouser, Oil-Well Cement and C3S Hydration Under High Pressure as Seen by In Situ X-Ray Diffraction, Temperatures ≤80°C with No Additives, J. Am. Ceram. Soc. 94 (2011) 1591–1597. https://doi.org/10.1111/j.1551-2916.2010.04284.x.

[7] A.C. Jupe, A.P. Wilkinson, G.P. Funkhouser, The effect of pressure on tricalcium silicate hydration at different temperatures and in the presence of retarding additives, Cem. Concr. Res. 42 (2012) 1083–1087. https://doi.org/10.1016/J.CEMCONRES.2012.04.008.

[8] F. Lin, C. Meyer, Hydration kinetics modeling of Portland cement considering the effects of curing temperature and applied pressure, Cem. Concr. Res. 39 (2009) 255–265. https://doi.org/10.1016/j.cemconres.2009.01.014.

[9] X. Pang, C. Meyer, R. Darbe, G.P. Funkhouser, Modeling the Effect of Curing Temperature and Pressure on Cement Hydration Kinetics, ACI Mater. J. 110 (2013) 137–148. https://doi.org/10.14359/51685528.

[10] B. Bresson, F. Meducin, H. Zanni, C. Noik, Hydration of tricalcium silicate (C3S) at high

temperature and high pressure, J. Mater. Sci. 37 (2002) 5355–5365. https://doi.org/10.1023/A:1021093528888.

[11] M. Palou, V. Živica, T. Ifka, M. Boháč, M. Zmrzlý, Effect of hydrothermal curing on early hydration of G-Oil well cement, J. Therm. Anal. Calorim. 116 (2014) 597–603. https://doi.org/10.1007/s10973-013-3511-7.

[12] M.T. Palou, E. Kuzielová, M. Žemlička, M. Boháč, R. Novotný, The effect of curing temperature on the hydration of binary Portland cement: Slag and Portland cement—metakaolin-blended cements, J. Therm. Anal. Calorim. 125 (2016) 1301–1310. https://doi.org/10.1007/s10973-016-5395-9.

[13] M.T. Palou, E. Kuzielová, R. Novotný, F. Šoukal, M. Žemlička, Blended cements consisting of Portland cement–slag–silica fume–metakaolin system, J. Therm. Anal. Calorim. 125 (2016) 1025–1034. https://doi.org/10.1007/s10973-016-5399-5.

[14] E. Kuzielová, M. Žemlička, J. Másilko, M.T. Palou, Pore structure development of blended G-oil well cement submitted to hydrothermal curing conditions, Geothermics. 68 (2017) 86–93. https://doi.org/10.1016/J.GEOTHERMICS.2017.03.001.

[15] M.S. Morsy, S.H. Alsayed, M. Aqel, Effect of Elevated Temperature on Mechanical Properties and Microstructure of Silica Flour Concrete, Int. J. Civ. Environ. Eng. 10 (2010) 1–5.

[16] M.T. Palou, F. Soukal, M. Bohac, P. Siler, T. Ifka, V. Zivica, Performance of G-Oil Well cement exposed to elevated hydrothermal curing conditions, J. Therm. Anal. Calorim. 118 (2014) 865–874. https://doi.org/10.1007/s10973-014-3917-x.

[17] Z. Ge, X. Yao, X. Wang, W. Zhang, T. Yang, Thermal performance and microstructure of oil well cement paste containing subsphaeroidal konilite flour in HTHP conditions, Constr. Build. Mater. 172 (2018) 787–794. https://doi.org/10.1016/j.conbuildmat.2018.03.268.

[18] Z. Xie, X. Yao, influence of the particle size distribution of silica flour on the mechanical and microstructural properties of oil well cement paste exposed to HTHP conditions, Cer.-Silik. 63 (2019) 239–247. https://doi.org/10.13168/cs.2019.0016.

[19] S. Shaw, S.M. Clark, C.M.B. Henderson, Hydrothermal formation of the calcium silicate hydrates, tobermorite (Ca5Si6O16(OH)2 · 4H2O) and xonotlite (Ca6Si6O17(OH)2): An in situ synchrotron study, in: Chem. Geol., Elsevier, 2000: pp. 129–140. https://doi.org/10.1016/S0009-2541(99)00205-3.

[20] R. Jauberthie, M. Temimi, M. Laquerbe, Hydrothermal transformation of tobermorite gel to 10 Å tobermorite, Cem. Concr. Res. 26 (1996) 1335–1339. https://doi.org/10.1016/0008-8846(96)00122-6.

[21] J.R. Houston, R.S. Maxwell, S.A. Carroll, Transformation of meta-stable calcium silicate hydrates to tobermorite: Reaction kinetics and molecular structure from XRD and NMR spectroscopy, Geochem. Trans. 10 (2009) 1–14. https://doi.org/10.1186/1467-4866-10-1.

[22] S. Bahafid, S. Ghabezloo, M. Duc, P. Faure, J. Sulem, Effect of the hydration temperature on the microstructure of Class G cement: C-S-H composition and density, Cem. Concr. Res. 95 (2017) 270–281. https://doi.org/10.1016/j.cemconres.2017.02.008.

[23] K.J. Krakowiak, J.J. Thomas, S. James, M. Abuhaikal, F.J. Ulm, Development of silica-enriched cement-based materials with improved aging resistance for application in high-temperature environments, Cem. Concr. Res. 105 (2018) 91–110. https://doi.org/10.1016/j.cemconres.2018.01.004.

[24] L.H. Eilers, R.L. Root, Long-Term Effects of High Temperature on Strength Retrogression of Cements, in: SPE Calif. Reg. Meet., Society of Petroleum Engineers, 1976: p. 5028. https://doi.org/10.2118/5871-MS.

[25] E. Kuzielová, M. Žemlička, J. Másilko, M.T. Palou, Effect of additives on the performance of Dyckerhoff cement, Class G, submitted to simulated hydrothermal curing, J. Therm. Anal. Calorim. 133 (2018) 63–76. https://doi.org/10.1007/s10973-017-6806-2.

[26] E. Kuzielová, M. Žemlička, J. Másilko, M.T. Palou, Development of G-oil well cement phase composition during long therm hydrothermal curing, Geothermics. 80 (2019) 129–137.

https://doi.org/10.1016/J.GEOTHERMICS.2019.03.002.

[27] Y. Bu, J. Du, S. Guo, H. Liu, C. Huang, Properties of oil well cement with high dosage of metakaolin, Constr. Build. Mater. 112 (2016) 39–48. https://doi.org/10.1016/j.conbuildmat.2016.02.173.

[28] S. Ma, T. Yu, Y. Wang, M. Chaouche, S. Kawashima, Phase Evolution of Oil Well Cements with Nano-additive at Elevated Temperature/Pressure, ACI Mater. J. 113 (2016) 571–578. https://doi.org/10.14359/51689104.

[29] E. Fraga, J.D. Zea-Garcia, A. Yáñez, A.G. De La Torre, A. Cuesta, R. Valcárcel-Fernández, F. Farré-París, M. Malfois, M.A.G. Aranda, High-pressure and -temperature spinning capillary cell for in situ synchrotron X-ray powder diffraction, J. Synchrotron Radiat. 26 (2019) 1238–1244. https://doi.org/10.1107/S1600577519005150.

[30] E. Fraga, A. Cuesta, J. Zea-Garcia, A. De la Torre, A. Yáñez-Casal, M. Aranda, Rietveld Quantitative Phase Analysis of Oil Well Cement: In Situ Hydration Study at 150 Bars and 150 °C, Materials (Basel). 12 (2019) 1897. https://doi.org/10.3390/ma12121897.

[31] E. Broni-bediako, O.F. Joel, G. Ofori-sarpong, Oil Well Cement Additives : A Review of the Common Types, Oil Gas Res. 2 (2016) 1000112. https://doi.org/10.4172/ogr.1000112.

[32] A. Cuesta, M.A.G. Aranda, J. Sanz, A.G. De La Torre, E.R. Losilla, Mechanism of stabilization of dicalcium silicate solid solution with aluminium, Dalt. Trans. 43 (2014). https://doi.org/10.1039/c3dt52194j.

[33] F. Canonico, Special binders as an alternative to Portland cement, in: 20th Int. Conf. Build. Mater., Weimar, 2018.

[34] J.B. González, N. González, C. Colldelram, L. Ribó, A. Fontserè, G. Jover-Manas, J. Villanueva, M. Llonch, G. Peña, A. Gevorgyan, Y. Nikitin, J.C. Martínez, C. Kamma-Lorger, E. Solano, I. Sics, S. Ferrer, M. Malfois, NCD-SWEET BEAMLINE UPGRADE, in: Mech. Eng. Des. Synchrotron Radiat. Equip. Instrum., Paris, 2018.

[35] G. Ashiotis, A. Deschildre, Z. Nawaz, J.P. Wright, D. Karkoulis, F.E. Picca, J. Kieffer, The fast azimuthal integration Python library: *pyFAI*, J. Appl. Crystallogr. 48 (2015) 510–519. https://doi.org/10.1107/S1600576715004306.

[36] R.B. Von Dreele, A.C. Larson, General structure analysis system (GSAS), Los Alamos Natl. Lab. Rep. LAUR. 748 (2004) 86–748.

[37] P. Thompson, D.E. Cox, J.B. Hastings, Rietveld Refinement of Debye-Scherrer Synchrotron X-ray Data from A1203, J. Appl. Crystallogr. 20 (1987) 79–83. https://doi.org/10.1107/S0021889887087090.

[38] W.A. Dollase, Correction of intensities of preferred orientation in powder diffractometry: application of the march model, J. Appl. Crystallogr. 19 (1986) 267–272. https://doi.org/10.1107/S0021889886089458.

[39] A.C. Jupe, A.P. Wilkinson, K. Luke, G.P. Funkhouser, Class H cement hydration at 180 °C and high pressure in the presence of added silica, Cem. Concr. Res. 38 (2008) 660–666. https://doi.org/10.1016/j.cemconres.2007.12.004.

[40] L.B. McCusker, R.B. Von Dreele, D.E. Cox, D. Louër, P. Scardi, Rietveld refinement guidelines, J. Appl. Crystallogr. 32 (1999) 36–50. https://doi.org/10.1107/S0021889898009856.

[41] M.A.G. Aranda, A.G. De la Torre, L. Leon-Reina, Rietveld Quantitative Phase Analysis of OPC Clinkers, Cements and Hydration Products, Rev. Mineral. Geochemistry. 74 (2012) 169–209. https://doi.org/10.2138/rmg.2012.74.5.

[42] A.G. De La Torre, S. Bruque, M.A.G. Aranda, Rietveld quantitative amorphous content analysis, J. Appl. Crystallogr. 34 (2001) 196–202. https://doi.org/10.1107/S0021889801002485.

[43] L. Nicoleau, A. Nonat, D. Perrey, The di- and tricalcium silicate dissolutions, Cem. Concr. Res. 47 (2013) 14–30. https://doi.org/10.1016/j.cemconres.2013.01.017.

Figure 1

Click here to access/download;Figure;Fig 1.TIF

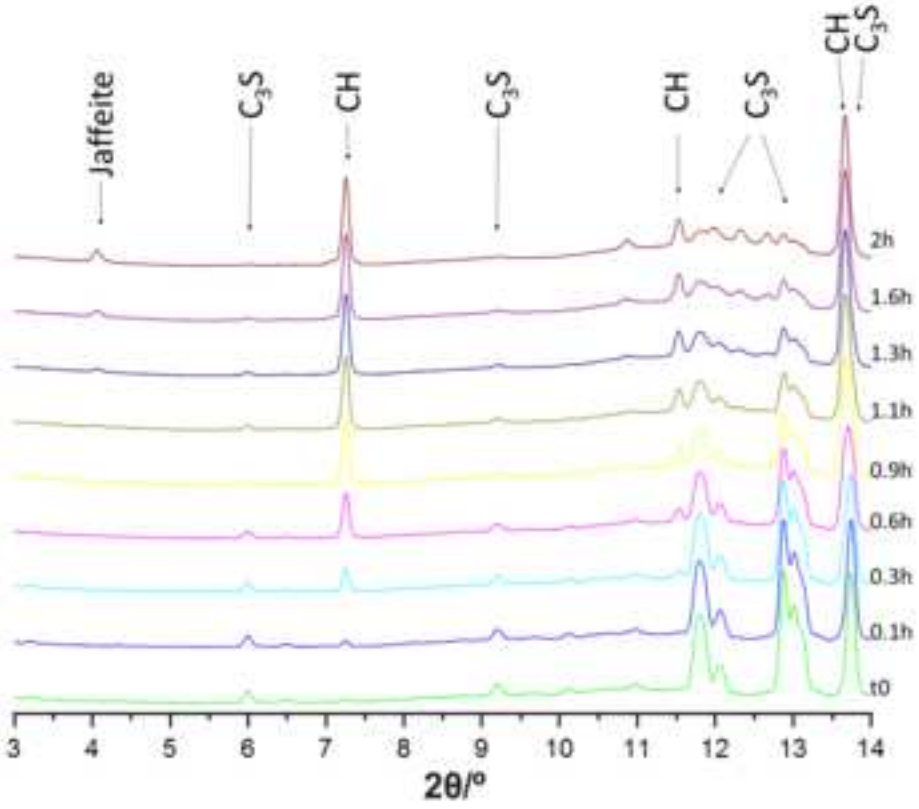

Figure 2

Click here to access/download;Figure;Fig 2.TIF

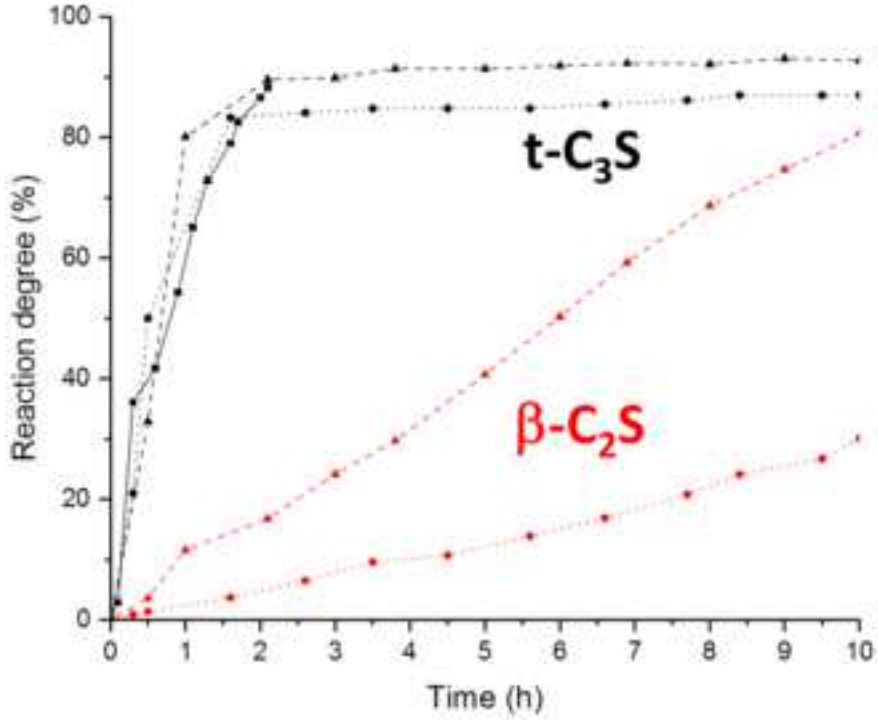

Figure 3

Click here to access/download;Figure;Fig 3.TIF

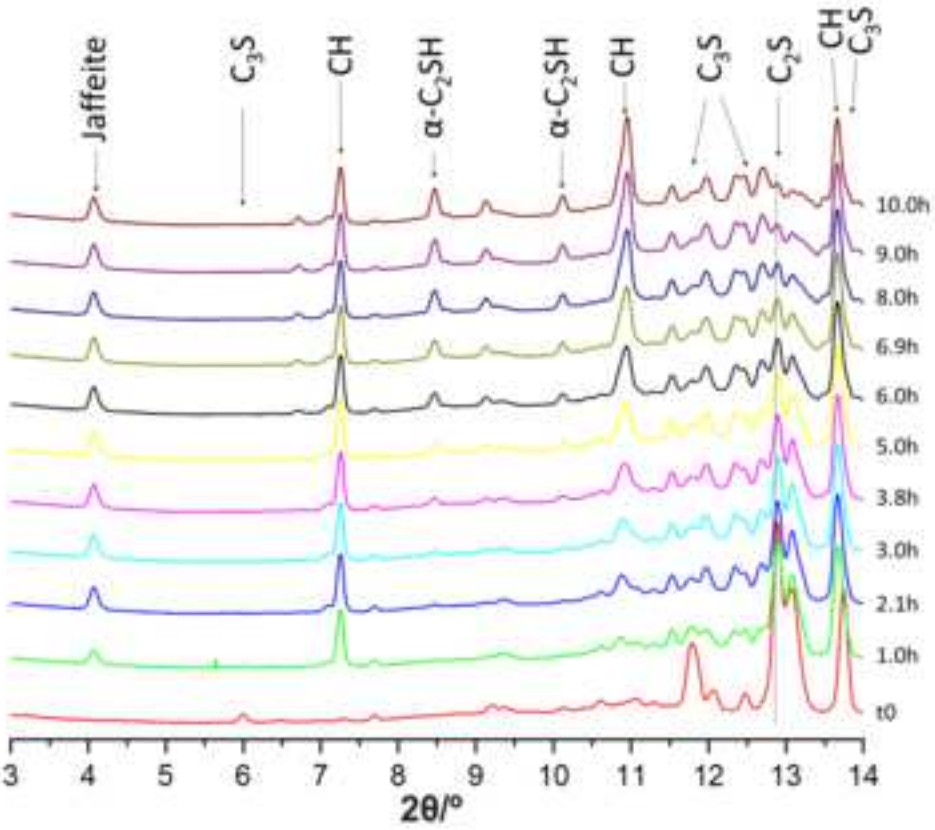

Figure 4

Click here to access/download;Figure;Fig 4.TIF

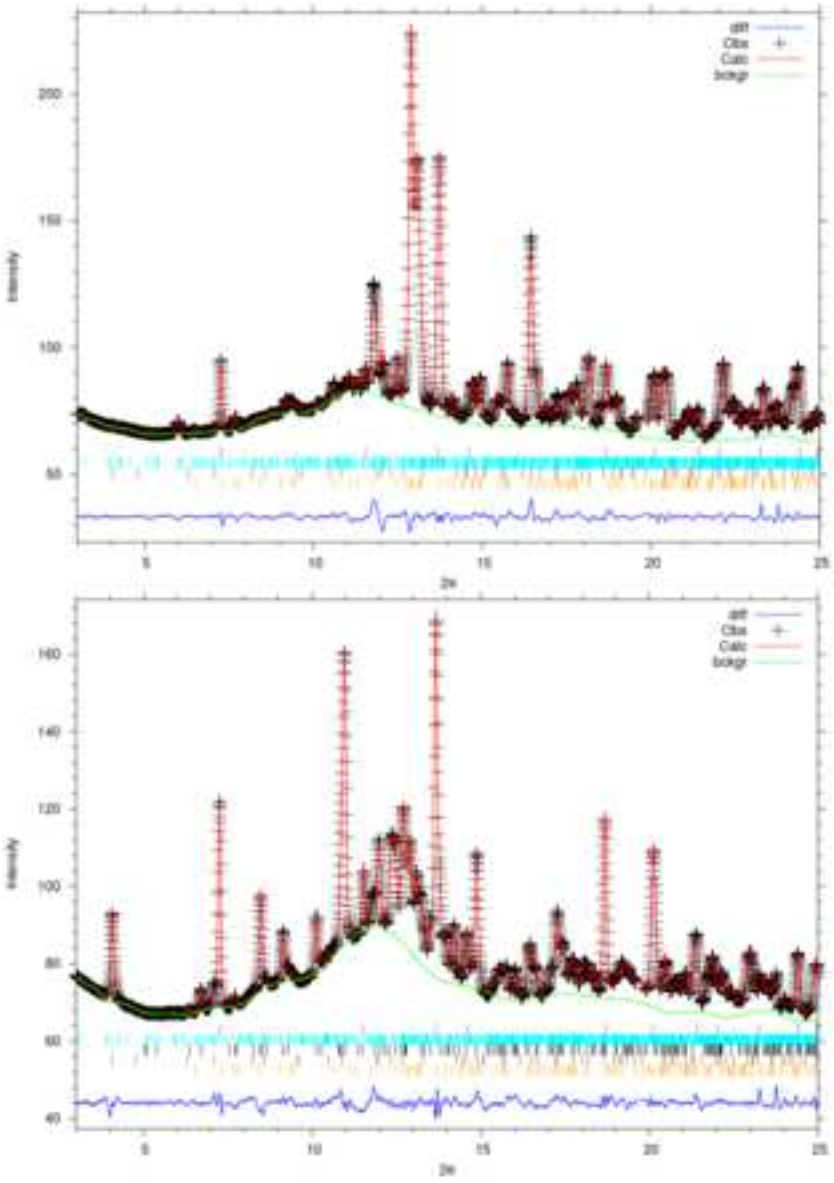

Figure 5

Click here to access/download;Figure;Fig 5.TIF

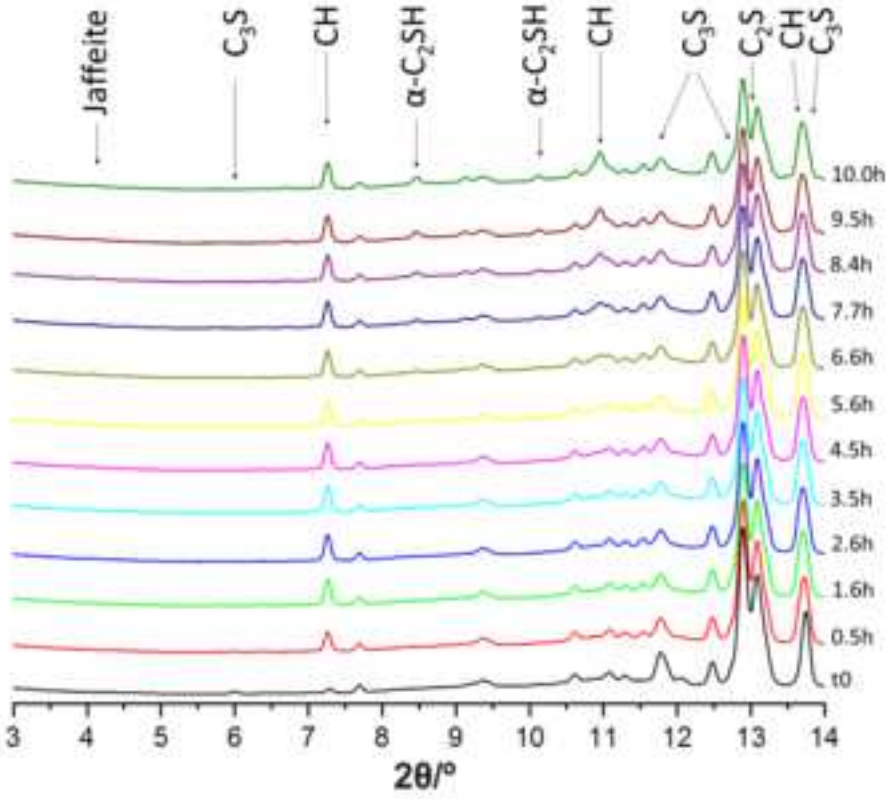

Figure 6

Click here to access/download;Figure;Fig 6.TIF

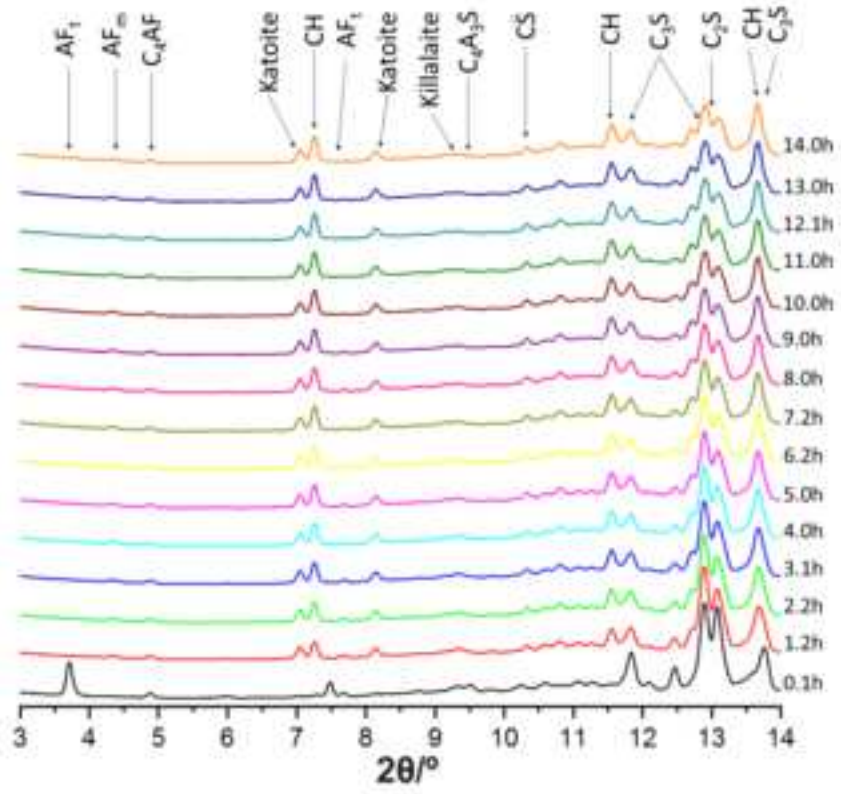

Supporting information accompanying the publication

Belite hydration at high temperature and pressure by in situ synchrotron powder diffraction

Alejandro Morales-Cantero[1], Angeles G. De la Torre[1], Ana Cuesta[1], Edmundo Fraga-Lopez[2], Shiva Shirani[1], Miguel A.G. Aranda[1,*]

[1]*Departamento de Química Inorgánica, Cristalografía y Mineralogía, Universidad de Málaga, Málaga, 29071, Spain.*

[2]*ALBA Synchrotron, Carrer de la Lum, 2-26, 08290 Cerdanyola del Vallès, Barcelona, Spain.*

** email: g_aranda@uma.es*

This supporting information includes:

Figures

Fig. S1. Laboratory powder X-ray diffraction Rietveld plot (λ=1.5406 Å) for crystalline I_2.

Fig. S2. Particle size distribution and cumulative volumetric particle size distribution for t-C_3S, β-C_2S and BC samples.

Fig. S3. Laboratory powder X-ray diffraction Rietveld plot (λ=0.7093 Å) for anhydrous t-C_3S.

Fig. S4. Laboratory powder X-ray diffraction Rietveld plot (λ=0.7093 Å) for anhydrous β-C_2S.

Fig. S5. Laboratory powder X-ray diffraction Rietveld plot (λ=0.7093 Å) for anhydrous BC.

Fig. S6. (Top) Selected *in situ* (T=RT and P=185 bars) synchrotron powder X-ray diffraction Rietveld plot for crystalline I_2. (Bottom) Second-order (K'=4.0) Birch-Murnaghan equation of state fitting for the unit cell data of I_2 with increasing (red) and decreasing (blue) pressures.

Fig. S7. *In situ* synchrotron powder X-ray diffraction Rietveld plots for the t-C_3S paste hydrating under 180 bars and 160ºC at (top) t_0 and (bottom) 2 hours.

Fig. S8. Selected low angle range of SXRPD raw patterns for the β-C_2S paste collected at 180 bars and 120ºC as a function of hydration time. The inset shown an enlarged view to highlight that β-C_2S does not react in the studied time range.

Fig. S9. *In situ* synchrotron powder X-ray diffraction Rietveld plots for the 20 wt% t-C_3S and 80 wt% β-C_2S paste hydrating under 180 bars and 160ºC at (top) t_0 and (bottom) 8.4 hours.

Fig. S10. *In situ* synchrotron powder X-ray diffraction Rietveld plots for belite cement paste hydrating under 180 bars and 155ºC at (top) 1.2 and (bottom) 14 hours.

Tables

Table S1. Rietveld quantitative phase analysis for anhydrous BC sample from laboratory X-ray powder diffraction.

Table S2. Elemental composition for the BC sample used in this study.

Table S3. Phase scale factors obtained from the Rietveld analyses for the t-C_3S paste at increasing hydration times under 180 bars and 160 ºC. The degree of reaction for t-C_3S is also given which is derived from the ratios of its scale factor and that at t_0.

Table S4. Phase scale factors obtained from the Rietveld analyses for the 50 wt% t-C_3S and 50 wt% β-C_2S paste after selected hydration times under 180 bars and 160 ºC. The degree of reaction for t-C_3S and β-C_2S are also given.

Table S5. Phase scale factors obtained from the Rietveld analysis for the t-C_3S and β-C_2S phases in the 20 wt% t-C_3S and 80 wt% β-C_2S paste at increasing hydration times under 180 bars and 160 ºC. The degree of reaction for t-C_3S and β-C_2S are also given.

Table S6. Phase scale factors obtained from the Rietveld analyses for the belite cement paste at increasing hydration times under 180 bars and 155 ºC. The degree of reaction for t-C_3S and β-C_2S are also given.

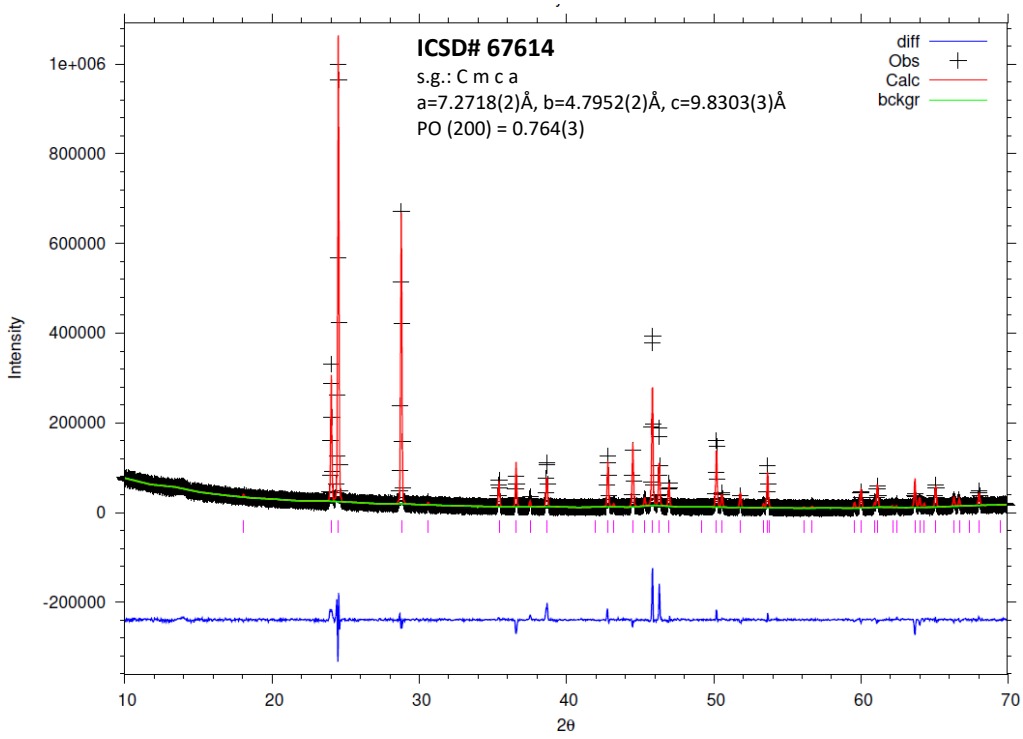

Fig. S1. Laboratory powder X-ray diffraction Rietveld plot (λ=1.5406 Å) for crystalline I_2.

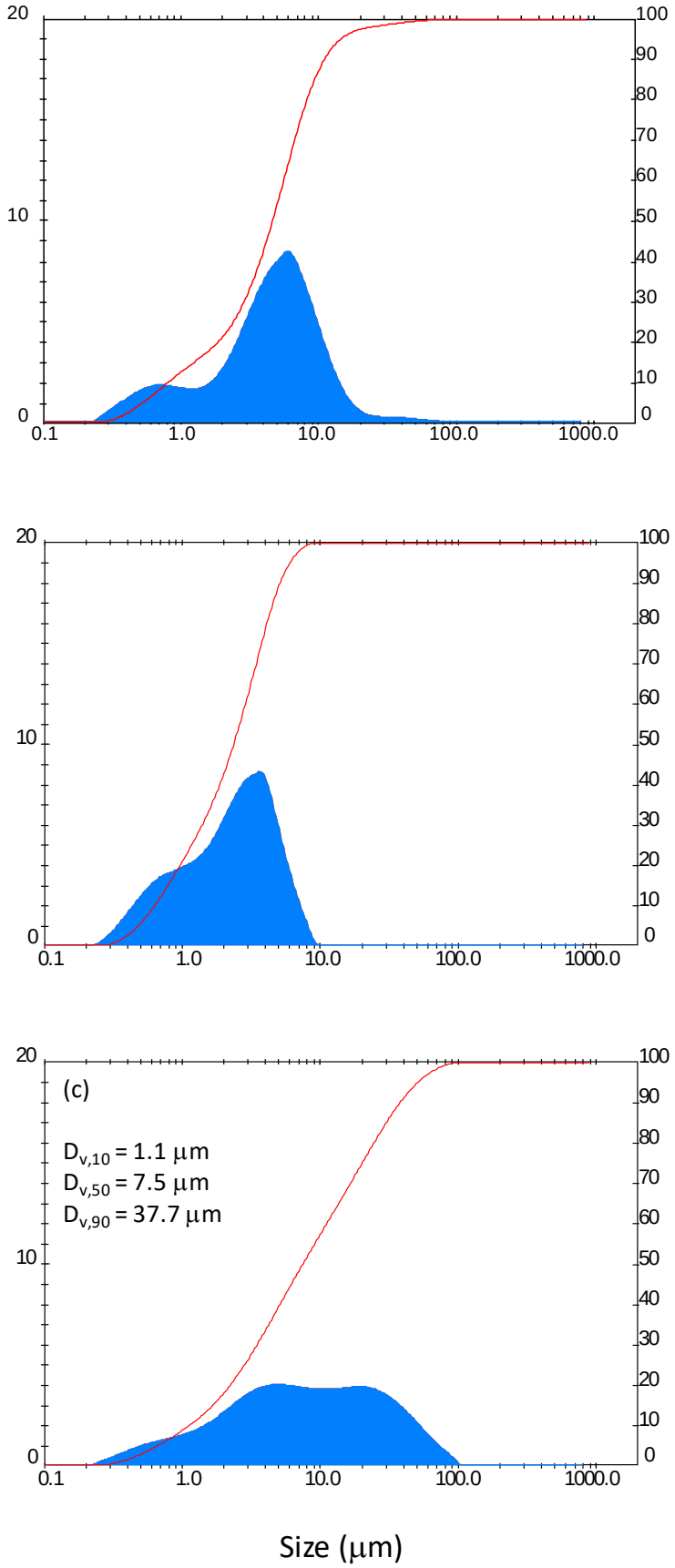

Fig. S2. Particle size distribution and cumulative volumetric particle size distribution for t-C_3S, β-C_2S and BC samples.

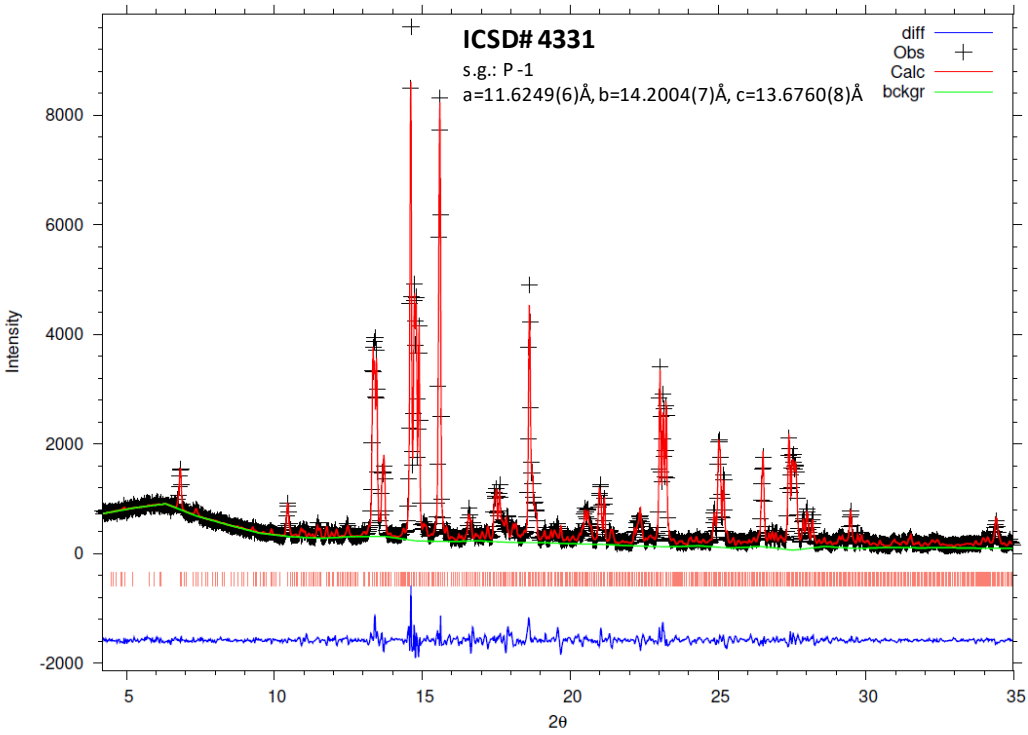

Fig. S3. Laboratory powder X-ray diffraction Rietveld plot (λ=0.7093 Å) for anhydrous t-C_3S.

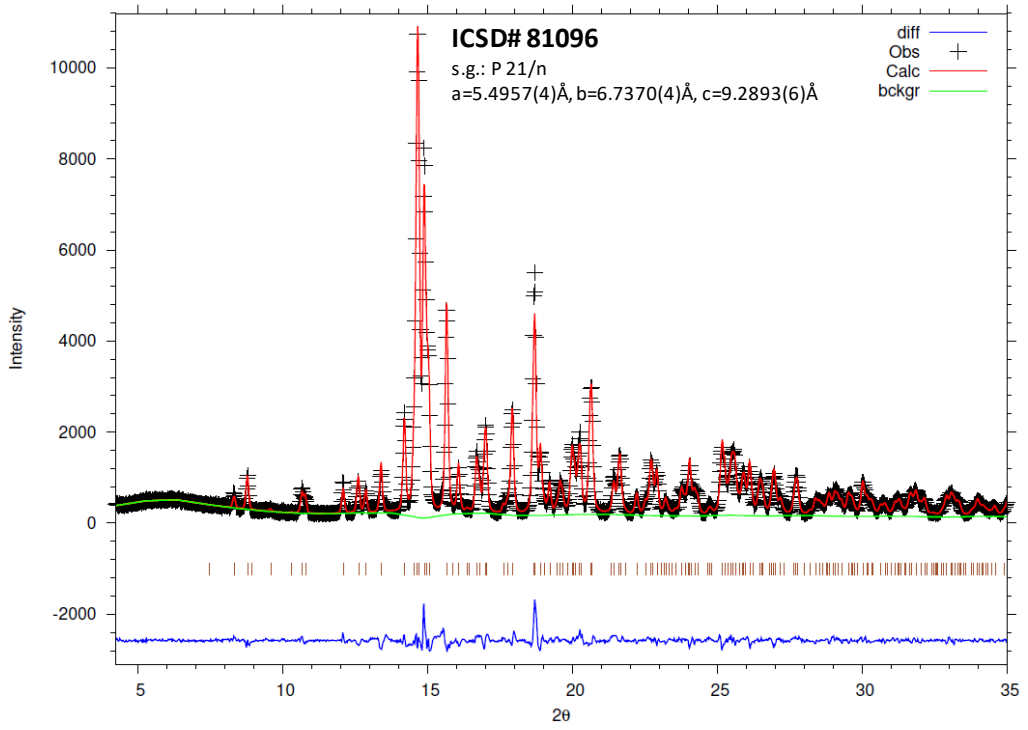

Fig. S4. Laboratory powder X-ray diffraction Rietveld plot (λ=0.7093 Å) for anhydrous β-C_2S.

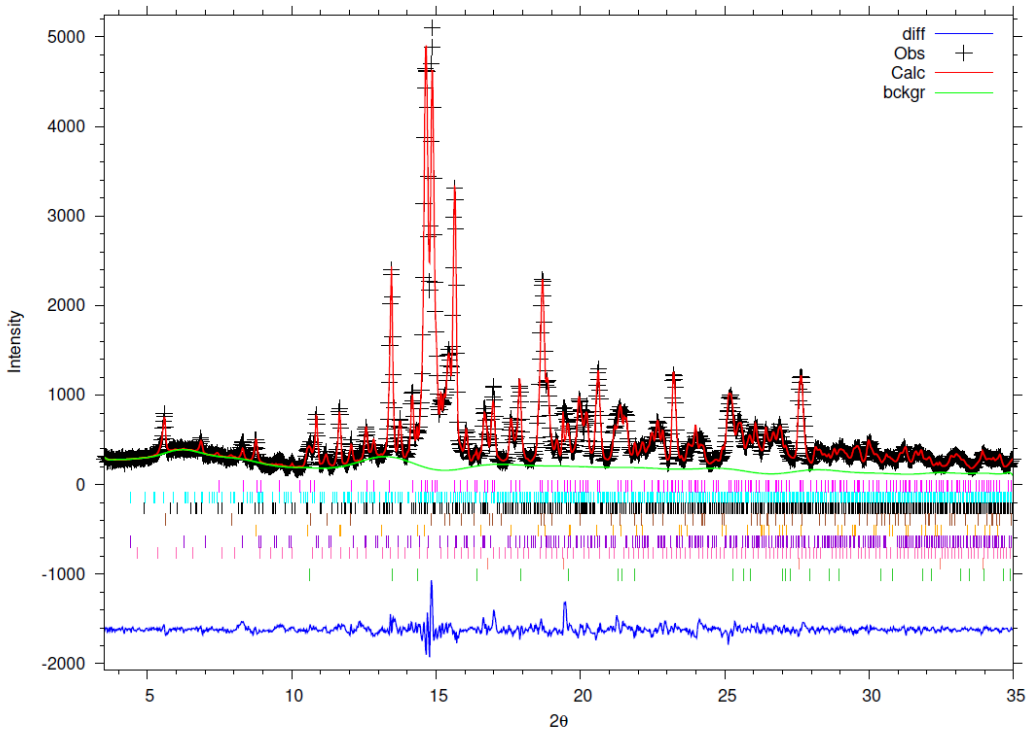

Fig. S5. Laboratory powder X-ray diffraction Rietveld plot (λ=0.7093 Å) for anhydrous BC.

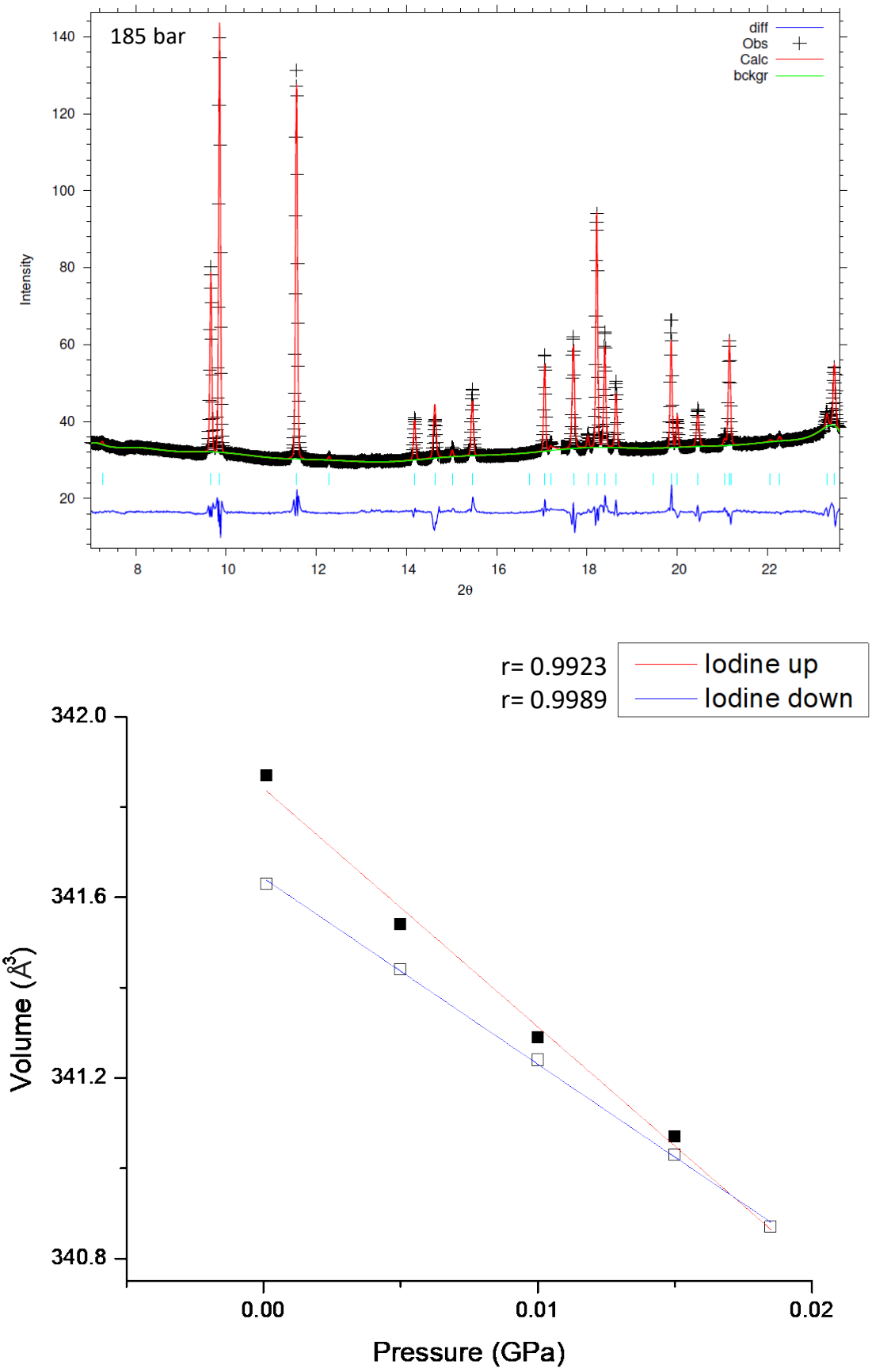

Fig. S6. (Top) Selected *in situ* (T=RT and P=185 bars) synchrotron powder X-ray diffraction Rietveld plot for crystalline I_2. (Bottom) Second-order (K'=4.0) Birch-Murnaghan equation of state fitting for the unit cell data of I_2 with increasing (red) and decreasing (blue) pressures.

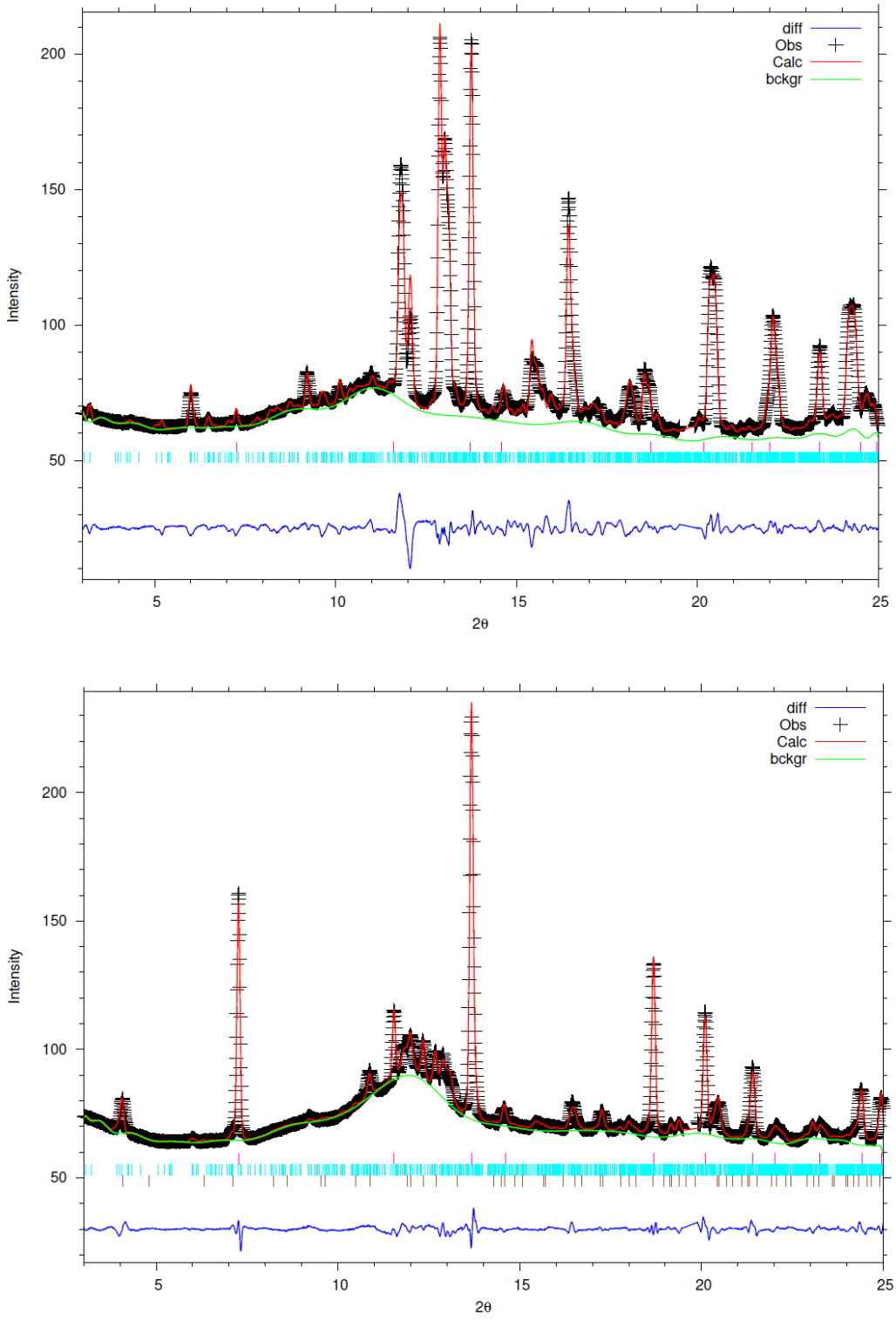

Fig. S7. *In situ* synchrotron powder X-ray diffraction Rietveld plots for the t-C_3S paste hydrating under 180 bars and 160ºC at (top) t_0 and (bottom) 2 hours.

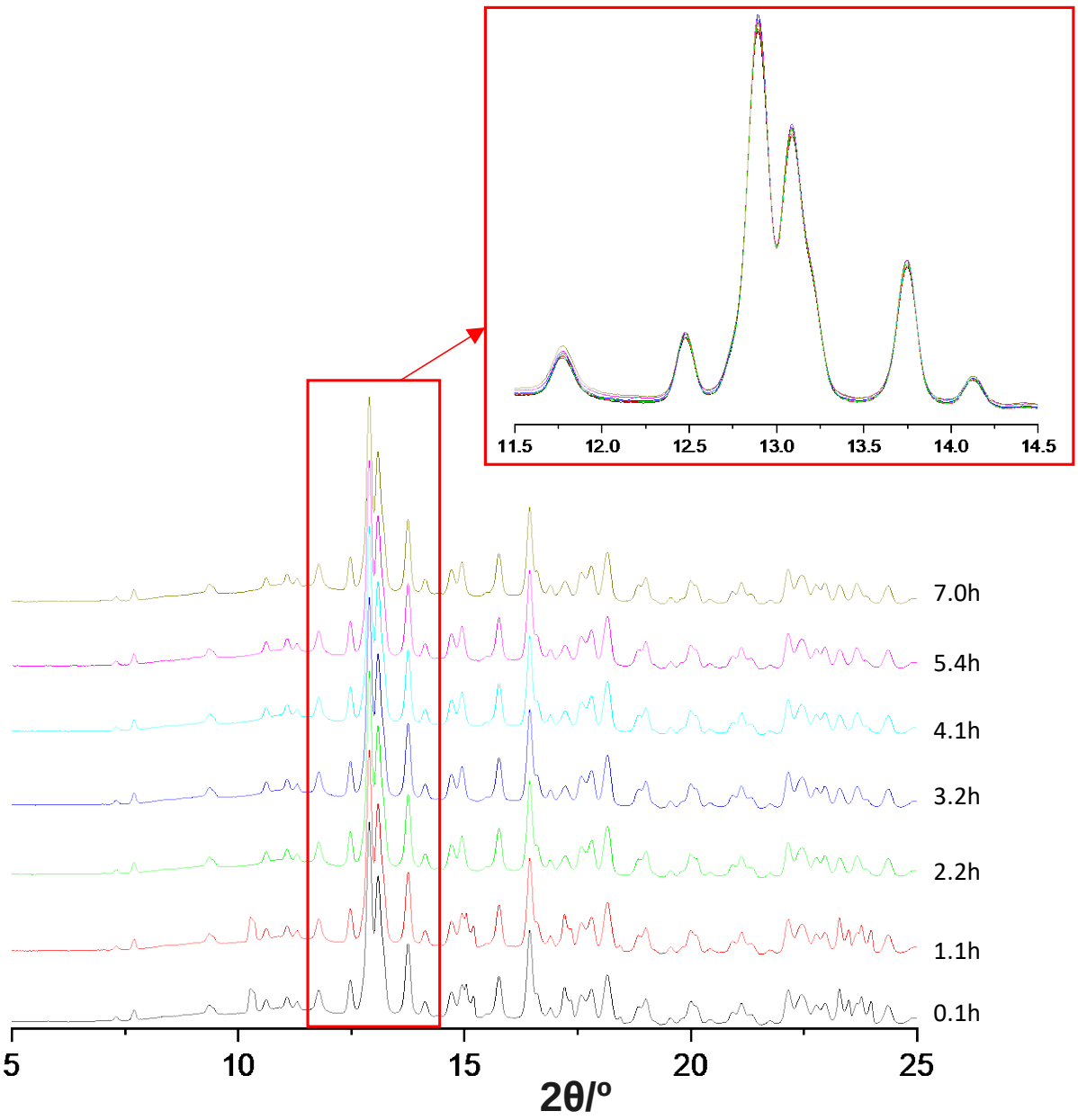

Fig. S8. Selected low angle range of SXRPD raw patterns for the β-C_2S paste collected at 180 bars and 120ºC as a function of hydration time. The inset shown an enlarged view to highlight that β-C_2S does not react in the studied time range.

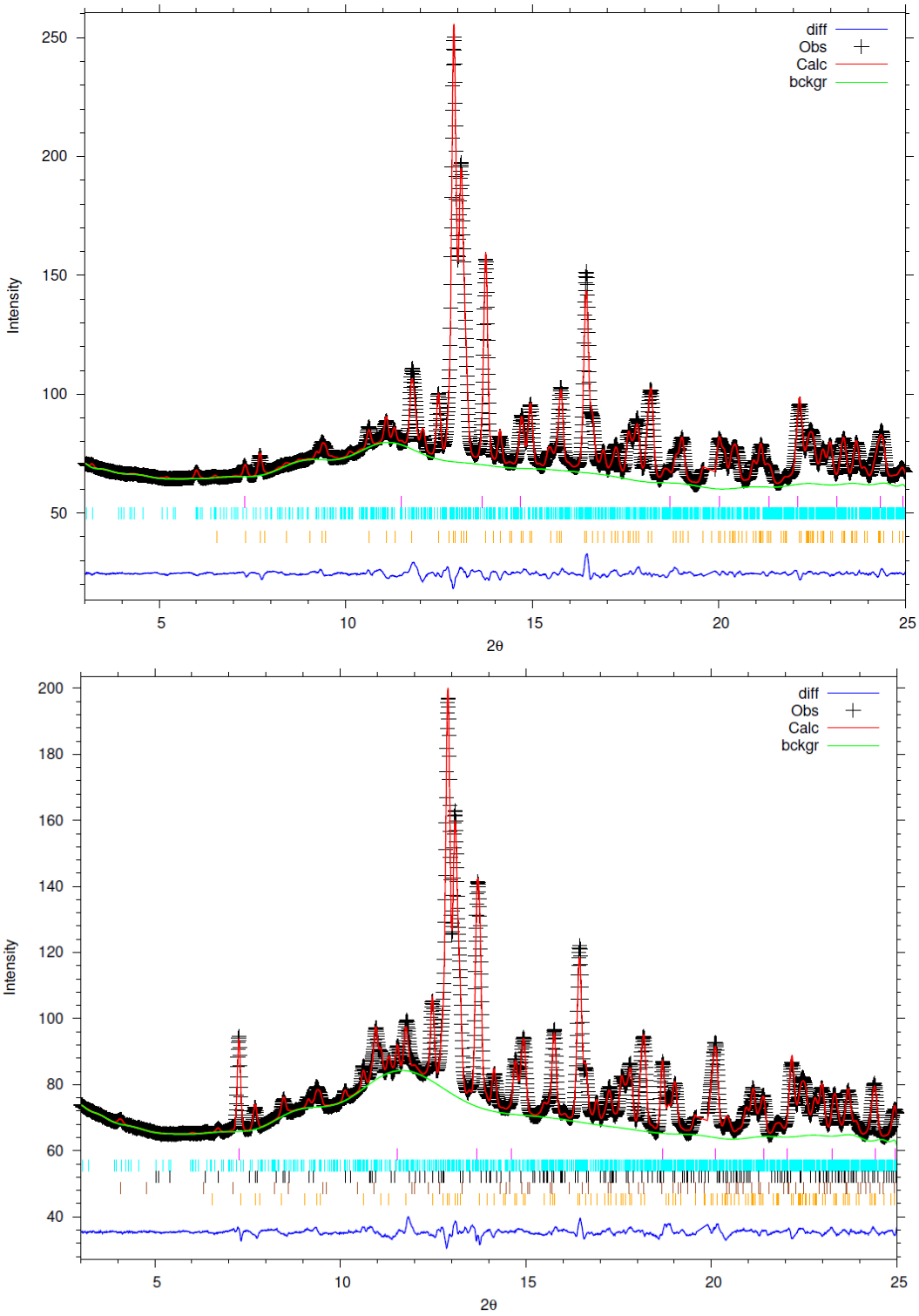

Fig. S9. *In situ* synchrotron powder X-ray diffraction Rietveld plots for the 20 wt% t-C_3S and 80 wt% β-C_2S paste hydrating under 180 bars and 160ºC at (top) t_0 and (bottom) 8.4 hours.

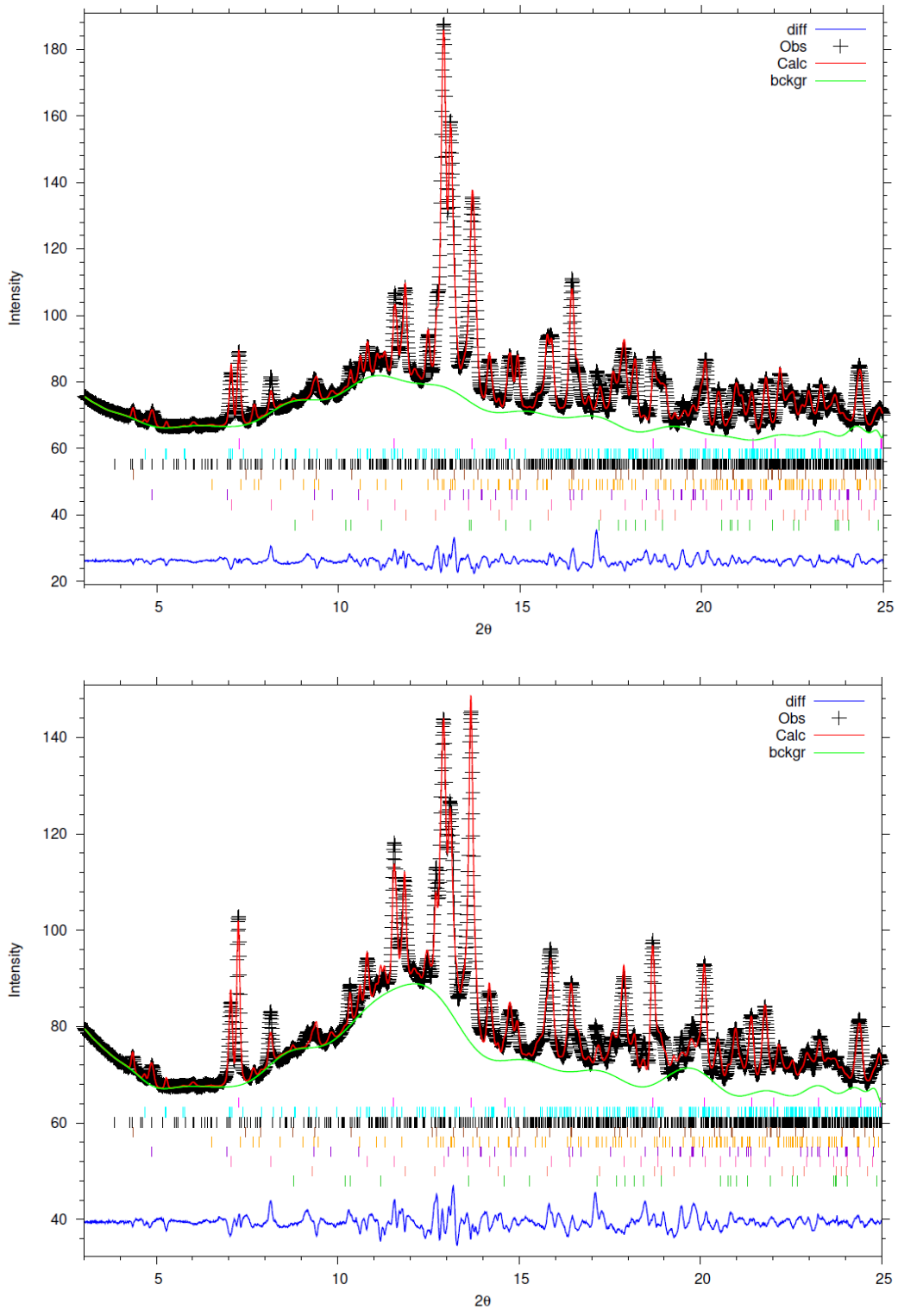

Fig. S10. *In situ* synchrotron powder X-ray diffraction Rietveld plots for belite cement paste hydrating under 180 bars and 155ºC at (top) 1.2 and (bottom) 14 hours.

Table S1. Rietveld quantitative phase analysis for anhydrous BC sample from laboratory X-ray powder diffraction.

	C_3S	β-C_2S	C_4AF	$C_4A_3\bar{S}$	C_3A	$C\bar{S}$	MgO	$C\bar{C}$
Weight Fraction (%)	25.2	53.7	12.2	2.4	1.2	2.1	1.3	1.9

Table S2. Elemental composition for the BC sample used in this study.

	CaO	SiO_2	SO_3	Al_2O_3	Fe_2O_3	MgO	K_2O	Na_2O	TiO_2	P	MnO	SrO	Others
Weight Fraction (%)	61.1	22.1	4.9	4.5	2.8	2.8	0.9	0.2	0.2	0.1	0.1	0.1	0.2

Table S3. Phase scale factors (S_{ph}) obtained from the Rietveld analyses for the t-C_3S paste at increasing hydration times under 180 bars and 160 ºC. The degree of reaction (α) for t-C_3S is also given which is derived from the ratios of its scale factor and that at t_0.

	Time (h)										
	0.0	**0.1**	**0.3**	**0.6**	**0.9**	**1.1**	**1.3**	**1.6**	**1.7**	**2.0**	**2.1**
α (%) t-C_3S	0.0	2.9	36.1	41.8	54.3	65.1	72.9	79.0	82.5	86.6	88.3
S_{ph} t-C_3S	0.0582	0.0565	0.0372	0.0339	0.0266	0.0203	0.0158	0.0122	0.0102	0.0078	0.0068
S_{ph} CH	0.0349	0.0736	0.4116	0.4159	0.5873	0.6724	0.7434	0.7819	0.7863	0.7991	0.7982
S_{ph} Jaffeite	0.0000	0.0000	0.0000	0.0000	0.0000	0.0031	0.0046	0.0074	0.0116	0.0220	0.0252

Table S4. Phase scale factors (S_{ph}) obtained from the Rietveld analyses for the 50 wt% t-C_3S and 50 wt% β-C_2S paste after selected hydration times under 180 bars and 160 ºC. The degrees of reaction (α) for t-C_3S and β-C_2S are also given.

	Time (h)											
	0.0	**0.5**	**1.0**	**2.1**	**3.0**	**3.8**	**5.0**	**6.0**	**6.9**	**8.0**	**9.0**	**10.0**
α (%) t-C_3S	0.0	32.9	80.1	89.6	89.9	91.4	91.4	91.9	92.3	92.2	93.1	92.8
α (%) β-C_2S	0.0	3.6	11.6	16.8	24.2	29.7	40.7	50.3	59.3	68.7	74.7	80.7
S_{ph} t-C_3S	0.0347	0.0233	0.0069	0.0036	0.0035	0.0030	0.0030	0.0028	0.0027	0.0027	0.0024	0.0025
S_{ph} β-C_2S	0.1866	0.1798	0.1649	0.1553	0.1415	0.1311	0.1106	0.0928	0.0760	0.0584	0.0473	0.0361
S_{ph} CH	0.0000	0.2256	0.4090	0.4171	0.4156	0.4136	0.4147	0.4155	0.4164	0.4118	0.4102	0.4067
S_{ph} Jaffeite	0.0000	0.0018	0.0246	0.0334	0.0339	0.0338	0.0337	0.0333	0.0334	0.0345	0.0331	0.0341
S_{ph} α-C_2SH	0.0000	0.0000	0.0000	0.0058	0.0103	0.0148	0.0232	0.0341	0.0388	0.0509	0.0535	0.0646

Table S5. Phase scale factors (S_{ph}) obtained from the Rietveld analysis for the t-C_3S and β-C_2S phases in the 20 wt% t-C_3S and 80 wt% β-C_2S paste at increasing hydration times under 180 bars and 160 ºC. The degrees of reaction (α) for t-C_3S and β-C_2S are also given.

	Time (h)												
	0.0	**0.3**	**0.5**	**1.6**	**2.6**	**3.5**	**4.5**	**5.6**	**6.6**	**7.7**	**8.4**	**9.5**	**10.0**
α (%) t-C_3S	0.0	21.0	50.0	83.3	84.1	84.8	84.8	84.8	85.5	86.2	87.0	87.0	87.0
α (%) β-C_2S	0.0	0.9	1.4	3.7	6.5	9.6	10.7	13.9	16.9	20.8	24.1	26.7	30.1
S_{ph} t-C_3S	0.0138	0.0109	0.0069	0.0023	0.0022	0.0021	0.0021	0.0021	0.0020	0.0019	0.0018	0.0018	0.0018
S_{ph} β-C_2S	0.2895	0.2870	0.2854	0.2789	0.2707	0.2618	0.2585	0.2492	0.2407	0.2292	0.2196	0.2122	0.2025
S_{ph} CH	0.0196	0.0760	0.1585	0.2105	0.2137	0.2128	0.2187	0.2192	0.2181	0.2171	0.2162	0.2233	0.2192
S_{ph} Jaffeite	0.0000	0.0000	0.0000	0.0014	0.0016	0.0018	0.0020	0.0023	0.0024	0.0025	0.0025	0.0025	0.0023
S_{ph} α-C_2SH	0.0000	0.0000	0.0000	0.0000	0.0011	0.0016	0.0026	0.0040	0.0060	0.0088	0.0114	0.0163	0.0188

Table S6. Phase scale factors (S_{ph}) obtained from the Rietveld analyses for the belite cement paste at increasing hydration times under 180 bars and 155 ºC. The degrees of reaction (α) for t-C_3S and β-C_2S are also given.

	Time (h)															
	0.1	**0.7**	**1.2**	**2.2**	**3.1**	**4.0**	**5.0**	**6.2**	**7.2**	**8.0**	**9.0**	**10.0**	**11.0**	**12.1**	**13.0**	**14.0**
α (%) C_3S	0.0	33.9	48.4	53.2	56.5	58.1	58.1	59.7	59.7	59.7	59.7	59.7	59.7	59.7	59.7	59.7
α (%) C_2S	0.0	4.3	9.8	17.6	24.5	29.9	35.7	41.1	44.5	47.6	51.2	53.3	56.1	58.4	60.3	62.4
S_{ph} C_3S	0.0062	0.0049	0.0032	0.0029	0.0027	0.0026	0.0026	0.0025	0.0025	0.0025	0.0025	0.0025	0.0025	0.0025	0.0025	0.0025
S_{ph} C_2S	0.1740	0.1665	0.1570	0.1433	0.1313	0.1219	0.1118	0.1024	0.0966	0.0912	0.0849	0.0812	0.0764	0.0723	0.0691	0.0654
S_{ph} C_4AF	0.0175	0.0140	0.0138	0.0137	0.0136	0.0134	0.0135	0.0133	0.0135	0.0132	0.0132	0.0133	0.0133	0.0134	0.0132	0.0132
S_{ph} $C_4A_3\bar{S}$	0.0017	0.0000	0.0000	0.0000	0.0000	0.0000	0.0000	0.0000	0.0000	0.0000	0.0000	0.0000	0.0000	0.0000	0.0000	0.0000
S_{ph} $C\bar{S}$	0.0049	0.0040	0.0048	0.0054	0.0055	0.0056	0.0057	0.0060	0.0061	0.0056	0.0061	0.0061	0.0061	0.0062	0.0063	0.0063
S_{ph} $C\bar{C}$	0.0123	0.0100	0.0098	0.0098	0.0095	0.0095	0.0092	0.0089	0.0090	0.0088	0.0087	0.0087	0.0084	0.0085	0.0085	0.0084
S_{ph} MgO	0.0270	0.0289	0.0277	0.0271	0.0257	0.0250	0.0230	0.0230	0.0226	0.0217	0.0215	0.0212	0.0209	0.0202	0.0200	0.0196
S_{ph} CH	0.0000	0.1533	0.1844	0.2145	0.2248	0.2364	0.2429	0.2503	0.2596	0.2609	0.2666	0.2715	0.2744	0.2750	0.2791	0.2829
S_{ph} Killalaite	0.0000	0.0099	0.0130	0.0142	0.0144	0.0146	0.0150	0.0151	0.0154	0.0153	0.0155	0.0157	0.0156	0.0157	0.0157	0.0159
S_{ph} Katoite	0.0016	0.0134	0.0144	0.0152	0.0155	0.0158	0.0160	0.0160	0.0163	0.0162	0.0165	0.0164	0.0166	0.0164	0.0165	0.0164
S_{ph} AF_t	0.0026	0.0000	0.0000	0.0000	0.0000	0.0000	0.0000	0.0000	0.0000	0.0000	0.0000	0.0000	0.0000	0.0000	0.0000	0.0000
S_{ph} AF_m	0.0000	0.0011	0.0015	0.0017	0.0017	0.0017	0.0017	0.0018	0.0018	0.0018	0.0018	0.0018	0.0018	0.0017	0.0017	0.0018